



universität
wien

MASTERARBEIT MASTER THESIS

Titel der Masterarbeit / Title of the Master Thesis

“Fluorescence tomography data analysis of *in vivo*
biodistribution of near infrared dye labeled carriers”

Verfasst von / Submitted by
Vasilena Georgieva, BSc

Angestrebter akademischer Grad / In partial fulfilment of the requirements for the degree of
Master of Science (MSc)

Wien, 2020 / Vienna, 2020

Studienkennzahl lt. Studienblatt / Degree program code as
it appears on the student record sheet:

Studienrichtung lt. Studienblatt / Degree program as it
appears on the student record sheet:

Betreut von / Supervisor:

Mitbetreut von / Co-supervisor:

UA 066 606

Master's degree in Drug Discovery
and Development

Univ. Prof. Dipl. Ing. Dr. Manfred
Ogris

Haider Sami, PhD

Acknowledgment

I wish to express my sincere gratitude to Prof. Manfred Ogris who gave me the chance to gain experience and knowledge in Laboratory of Macromolecular Cancer Therapeutics (MMCT) and made my master thesis possible.

I sincerely thank my supervisor Dr. Haider Sami for his dedication, for the irreplaceable help he has given me, for his competent supervision and for his support during the time I was part of the MMCT team.

I also thank Mag. Simon Decker and Mag. Fatih Alioglu for their kind guidance.

I am thankful to the amazing students that I met in MMCT for the great working environment we created together and for the friendly support they always hung on me.

Last but not least, I would like to thank my father Ivan for making all this possible, to thank my mother Irena for her support and to thank my partner Radoslav for his patience, understanding and efforts to motivate me throughout this period.

Abbreviations

FLI	Fluorescence imaging
BG	Bacterial ghosts
AF750	Alexa Fluor 750
BLI	Bioluminescence imaging
CL	Chemiluminescence
Fluc	Firefly luciferase
CT	Computed tomography
MRI	Magnetic resonance imaging
CCD	Charge coupled device
GFP	Green fluorescence protein
RFP	Red fluorescence protein
NIR	Near infrared
FLIT	Fluorescence imaging tomography
DLIT	Diffuse luminescence imaging tomography
mRNA	Messenger RNA
siRNA	Small interfering RNA
PAMP	Pathogen-associated molecular patterns
DCs	Dendritic cells
TLR	Toll-like receptor
ROI	Region of interest
PCR	Polymerase Chain Reaction
SSO	Splice Switching Oligonucleotides

Table of Contents

1. Abstract	5
2. Introduction	7
2.1. In vivo imaging	7
2.2. Bacterial ghost.....	12
2.2.1. Bacterial ghosts as adjuvant particles	13
2.2.2. Bacterial ghosts as carrier.....	14
2.3. Small interfering RNA technology	16
3. Aim of thesis	18
4. Material and Methods	19
4.1. Bacterial ghost project.....	19
4.1.1. BG project - animals, intraperitoneal administration, imaging	19
4.1.2. BG project – data analysis	22
4.2. siRNA project	23
4.2.1. siRNA project – animals, intratracheal administration, imaging	23
4.2.2. siRNA project – data analysis.....	24
5. Results and Discussion.....	26
5.1. Bacterial Ghost biodistribution	26
5.1.1. Bacterial ghost biodistribution in non-tumor mice – 2 hours after administration	26
5.1.2. Bacterial ghost biodistribution in non-tumor mice – 1 hour and 24 hours after administration .	30
5.1.3. Bacterial ghost biodistribution in tumor bearing mice (24h after administration)	35
5.2. Biodistribution of siRNA	41
5.2.1. 2D fluorescence imaging of AF750-siRNA	42
5.2.2. 3D FLIT of AF750-siRNA	45
5.2.3. Organ Imaging of AF750-siRNA	48
6. Conclusion.....	51
7. ADDENDUM	53
7.1. Introduction	53
7.2. Background	55
7.2.1. Aim of the experiment.....	55
7.2.2. Gene information	55
7.2.3. Genotyping	58
7.3. Material and Methods.....	60
7.3.1. Gene extraction	60
7.3.2. Polymerase Chain Reaction	61
7.3.3. Agarose Gel Electrophoresis.....	62
7.4. Results and Discussion.....	63
7.4.1. Genotyping of Tg(SftpC Luc)line6	63
7.4.2. Genotyping of Tg(Thy1.Luc)line7	65
7.4.3. Genotyping of Tg(Luc705)line1050	67
7.5. Conclusion.....	70
8. References:	71

1. Abstract

This thesis brings together two separate projects focused on the *in vivo* biodistribution of near infrared dye AlexaFluor750 (AF750) labeled carriers – Bacterial ghosts and siRNA. BGs are empty coats of Gram-negative bacteria produced by controlled expression of lysis gene E of bacteriophage phiX174, provoking high interest because of the possibility to play a role of selective drug delivery system. In turn, siRNA is a short double-stranded non-coding RNA used for post-transcriptional gene silencing and it is known as one of the most important discovery reached in gene regulation field.

Analysis of imaging data from the 3D fluorescent imaging tomography method employed *in vivo* for tracking AF750-labeled bacterial ghosts and siRNA was considered in more detail by employing Living Image software. First part is devoted to the biodistribution of bacterial ghosts after intraperitoneal administration in tumor bearing and tumor-free mouse models and followed by Fluorescence imaging tomography (FLIT) at different time points. The investigation performed in tumor bearing animals uncovered very strong preferences of the BGs to the tumor associated tissues in the pancreatic region. In the absence of tumor, the ghosts demonstrate significant affinity for certain organs belonging to the gastrointestinal tract and also for the uterus region. The study revealed considerable limitations of the applied FLIT method. However, the conclusions reached were satisfactorily confirmed by the organ validation. Second part traces the spread of intratracheally administrated siRNA in non-tumor bearing mice. The experiment resulted in development of sufficient pattern for analysis of the data generated by 2D epi-fluorescence imaging method and 3D FLIT method and it was found that siRNA targets mainly the lungs and secondly the kidneys. The generated data could be used for further investigation with regard to delivery vectors and improvement of diagnostic methods.

Zusammenfassung

Diese Arbeit fasst zwei separate Projekte zusammen, die sich mit der *in vivo*-Bioverteilung des Nahinfrarot-Farbstoffs AlexaFluor750 (AF750) markierten Trägers - Bacterial ghosts (BGs) und siRNA - befassen. BGs sind leere Hüllen gramnegativer Bakterien, die durch die kontrollierte Expression des Lysegenes E des Bakteriophagen phiX174 hergestellt werden. Für die Forschung sind sie interessant, weil sie die Möglichkeit bieten, die Rolle eines selektiven Arzneimittelabgabesystems zu übernehmen. Die siRN ist eine kurze doppelsträngige nicht-kodierende RNA, die für das post-transkriptionelle Gen-Silencing verwendet wird und als eine der wichtigsten Entdeckungen auf dem Gebiet der Genregulation bekannt ist.

Die Analyse von Bildgebungsdaten der AF750-markierten BGs und siRNA aus der *in vivo* verwendeten 3D-Fluoreszenzbildgebungstomographie wurde durch den Einsatz von Living Image Software ergänzt und somit weiter vertieft. Der erste Teil der Arbeit befasst sich mit der Bioverteilung von BGs nach intraperitonealer Verabreichung in tumortragenden und tumorfreien Mausmodellen, gefolgt von der Fluoreszenzbildgebungstomographie (FLIT) zu verschiedenen Zeitpunkten. Die Untersuchung an tumortragenden Tieren deckte sehr starke Präferenzen der BGs für die tumorassoziierten Geweben im Pankreasbereich auf. In Abwesenheit eines Tumors zeigen die BGs eine signifikante Affinität zu bestimmten Organen des Magen-Darm-Traktes und auch zur Gebärmutterregion. Die Studie zeigte erhebliche Einschränkungen der angewandten FLIT-Methode. Die Schlussfolgerungen wurden jedoch durch die Organvalidierung zufriedenstellend bestätigt. Im zweiten Teil steht die Ausbreitung der intratracheal verabreichten siRNA bei nicht tumortragenden Mäusen im Fokus. Das Experiment führte zur Entwicklung eines geeigneten Musters für die Analyse der Daten, die durch das 2D-Epifluoreszenz-Bildgebungsverfahren und das 3D-FLIT-Verfahren erzeugt wurden, und es wurde festgestellt, dass siRNA hauptsächlich die Lunge und zweitens die Nieren angreift. Die generierten Daten könnten zur weiteren Untersuchung der Abgabevektoren und zur Verbesserung der Diagnosemethoden verwendet werden.

2. Introduction

It is well known that cancer plays enormous role in the social health and despite the significant efforts concentrated in cancer research, it is still one of the main global causes of death. The most commonly used current treatments show certain positive results, often they prolong the life span of the patients, but rarely this leads to an improvement in the quality of life. The limiting factors and shortcomings are based on the serious side effects, formation of metastatic lesions and the inability to diagnose earlier. Attempts to address these challenges have resulted in alternative delivery methods such as bacterial ghosts system and specific targeting methods such as siRNA technology.

2.1. In vivo imaging

To better understand the origin of diseases such as cancer, the gene expression or the behavior of pathogens intra-tissue and intracellular are essential. Application of different imaging systems and technologies is growing with significant rate and it has already become indispensable part of the research field and medical practice. Imaging systems such as computed tomography, CT or magnetic resonance imaging, MRI which give anatomic and physiological information are commonly known and involved in clinical and preclinical practice, also some molecular imaging technologies such as positron emission tomography, PET or single-photon emission computed tomography, SPECT are in clinical use. However, still there are molecular imaging systems with untapped potential which are currently in experimental use such as fluorescence imaging tomography, FLIT, bioluminescence imaging, BLI, diffuse luminescence imaging tomography, DLIT, fluorescence-mediated tomography, FMT and more (Condeelis & Weissleder, 2015). The great importance of the bioluminescence and fluorescence imaging systems is due to its adaptation to *in vivo* use and its developing ability to provide deeper information about biological and chemical processes in fully integrated living systems. However, still numerous of limitations remain, for example tissue absorption, scattering or autofluorescence, and a lot of imperfections need to be overcome before the method is ready to reach the point of routinely use in clinical and preclinical studies. (Frederic Leblond, Scott C. Davis, 2010)

Presumably, the biggest benefits of development of the innovative imaging systems are currently concentrated in oncology. Several macroscopic imaging technologies are used daily for the provision of anatomic and function information about different tumors. Consequently, the focus has already shifted to finding answer to bigger questions related to the molecular

machinery (Condeelis & Weissleder, 2015). Though it is worth paying attention to areas other than the direct cancer research where the developing techniques such as FLI also play increasing role. Up to date are all topics linked to the drug delivery systems, respectively the assessment of biodistribution of drug carriers, DNA or small interfering RNA is an important task which can be handled by dint of the already mentioned developing microscopic and intravital optical techniques.

Chemiluminescence is one of the best known and widely used detection techniques imposed since the second half of the last century and applied to high-throughput detection of analytes in the field of biochemical analysis. It is based on the process of emitting photons when electrons move from the excited state to the ground state as a result of undergoing a chemical reaction. The need for real-time monitoring of physiology and pathology processes has triggered the rapid expansion of the method and its inclusion in *in vivo* imaging. Although chemiluminescence imaging surpasses the traditional detection techniques by its higher sensitivity resulted from lack of need of an external light source, when it is up to *in vivo* application the method still suffers from certain limitations like weak tissue penetration and short timeliness. As a result, bioluminescence became one of the most common noninvasive *in vivo* tools (Yan, Shi, Song, & Bi, 2019). Bioluminescence can be defined as a natural production of light (luminescence) generated by a chemical reaction during which the enzyme (luciferase) oxidizes a substrate (luciferin) resulting in photon emission (Badr, 2014). The group of luciferases comprises numerous enzymes that catalyze light-generating chemical reactions in living organisms and some of them require cofactors such as ATP and Mg²⁺ for their activity. Despite the existence of wide range of luciferases only few of them are so far of interest for the researchers and are used in biomedical research (Badr & Tannous, 2011). The most prevalently used for mammalian expression is firefly luciferase (Fluc). The identification and optimization of its DNA coding sequence resulted in ability of genetical introduction of the luciferase-expressing cassette into viruses, cancer cells or bearing transgenic animals for the needs of the bioluminescent imaging. Respectively the specificity of this natural phenomenon leads to the biggest advantage of the discussed method – its high specificity and sensitivity (Tseng, Vasquez, & Peterson, 2015). The bioluminescent reaction catalyzed by Fluc generates a yellow–green light with a peak emission at 562 nm and requires D-luciferin (a benzothiazole) as a substrate (Badr, 2014).

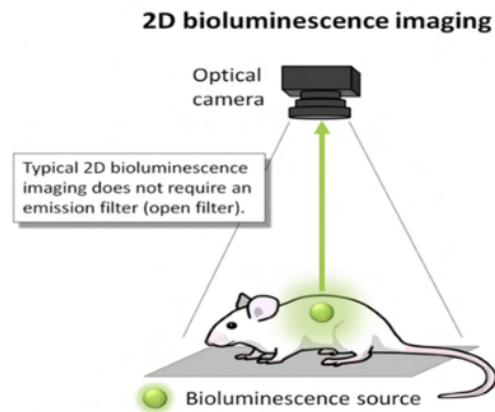


Fig.1. 2D Bioluminescence imaging (Tseng et al., 2015)

Although BLI is extremely suitable for pre-clinical evaluation of anti-cancer interventions, gene expression or cell growth and viability, it is still not the best approach when genetic modifications are not desirable, when expression of luciferase is not possible in particular model or when under investigation are biological changes or mechanisms underlying disease. In these cases, the preferable approach for generation of light signal is Fluorescence imaging (FLI) (Tseng et al., 2015).

Fluorescence imaging can be described as a technique which incorporates an external light source of appropriate wavelength for excitation of the fluorophores and a detection system (for example a charged coupled device CCD) with ability to achieve spectral and spatial separation to differentiate the emitted fluorescence from the fluorescence substances (Baert, 2008). The fluorescence probe could be genetically encoded reporting system or exogenous synthetic which are easier to handle and widely available and could be subdivided into small synthetic, organic and semiconductor solid-state nanoparticles (Stuker, Ripoll, Rudin, & Vouton, 2011). The exogenous imaging agents used in FLI are extremely specific for particular biological marker, they have its unique profile and fall in near-infrared spectrum, which leads to the need of broad range of excitation and emission filters to capture light from the visible to NIR spectrum (Tseng et al., 2015). Widely used examples for fluorescent reporters are Green fluorescent protein (GFP) and DsRed, with excitation wavelength of 470 nm and emission wavelength of 510 nm for GFP and respectively 560 nm and 580 nm for DsRed. The increment of the emission wavelength is proportional to the decrease of the tissue absorption because of the reduction of the attenuation of the light signal therefore for further depth penetration are required higher wavelength from the near-infrared region (Choy, Choyke, & Libutti, 2003). The NIR window can be roughly divided into two subgroups – (I)700-900nm range and (II) 1000-1700nm range. NIR I is the so-called ‘biological transparency NIR window’ and with

comparison to the visible spectrum it provides higher signal-to-background ratio by reducing scattering, autofluorescence and absorption which results in deeper tissue optical imaging. *In vivo* fluorescence imaging in NIR II outperforms NIR I window due to further reduction of the already mentioned characteristics but the field of research is much newer and in process of development, consequently the generation of long enough wavelength fluorescence emission in small-molecule organic dyes is still labored and the detection of the imaging systems is limited to 900-1000nm. Although a large number of fluorophores for different applications are available on the market (some of them even approved for clinical use such as indocyanine green and methylene blue), significant efforts are still being made to develop even more specific fluorophores or to improve already existing ones, for example probes with targeting ability for specific tissues and others which affords fast renal clearance have been synthesised (Hong, Antaris, & Dai, 2017).

The most simple and cost-effective FLI approach is the epi-illumination imaging. It differs from other approaches with the light source which could be appropriately filtered white light according to the suitable wavelength or laser source and with the position of this source which is at the same side as the detector reside. This technique is the most commonly used when it comes to surface imaging but it does not dispose of light propagation changes and reduction as a function of depth and of tissue optical properties (Baert, 2008).

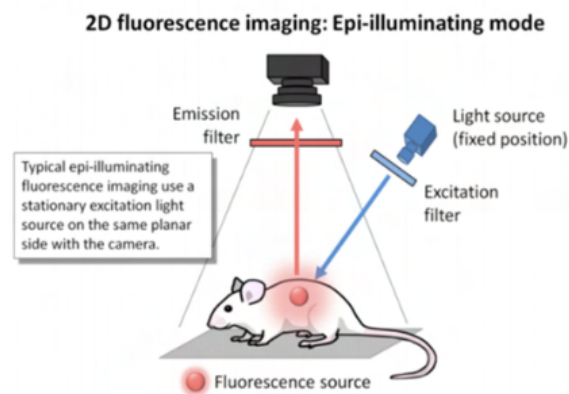


Fig.2. 2D Fluorescence imaging acquired by illuminating the surface (epi-illumination) (Tseng et al., 2015)

For achieving larger penetration depths can be used transillumination measurements during which the tissue crosses the light beam and signals first generate in the entire tissue before exciting on the other side of the animal and detected by the photon detector. However, both planar imaging strategies are limited to qualitative observations because of inability to resolve depth (Baert, 2008). The need of overcoming the limitations lead to introduction of tomography techniques such as fluorescence molecular tomography (FMT) for derivation of

quantitative information and mapping the three-dimensional distribution of the fluorescent probe (Stuker et al., 2011). The tomography approach uses a transillumination excitation light in adjustable position and close to the animal's body. The information received from the variety light source positions is combined with surface data produced by CT imaging and analyzed with aim to reconstruct a 3D distribution map of the probe of interest within the body (Tseng et al., 2015).

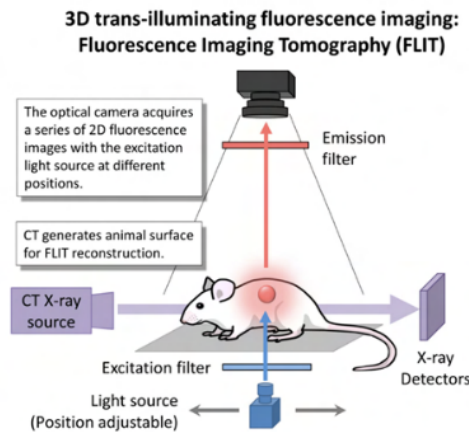


Fig.3. 3D Fluorescence imaging tomography (Tseng et al., 2015).

Despite the remarkable progress and the numerous opportunities provided by the whole-body fluorescence imaging a lot of limitations still remain and should be taken into consideration. Most common problems are caused by scattering events, absorption or autofluorescence. Using light in the NIR wavelength range partially solves the absorption issue and larger depths can be probed but still the absorption of oxyhaemoglobin, water and lipids should be considered. In addition, multiple scattering is the major mechanism for light propagation in the NIR imaging. Biomolecules such as NADH, tryptophan or elastin present in living tissue and can act as biochemical sources of autofluorescence, even though their impact can be neglected when it comes to far-red or NIR fluorescence imaging because most of the time the main excitation peaks for these fluorophores are in the visible part of the spectrum (Frederic Leblond, Scott C. Davis, 2010). Additionally, food fluorescence should be taken into account because it can strongly interfere with NIR agent imaging. The chlorophyll which is contained in the plant-based alfalfa food pellets commonly results in autofluorescence in the intestinal area and thereon an alfalfa-free diet is recommended (Tseng et al., 2015). The advancement in fluorescence imaging and more specific in fluorescence tomography is highly desired by reason of its multitudinous applications in pharmaceutical research. On first place the non-invasive imaging approach is widely used in the process of targets validation, for

example for visualization of receptors in tumors. On the other hand, another quite useful application is related to the examination of biodistribution and pharmacokinetics or even more – studying the drug-target interactions, for example checking if the drug reaches its molecular target or if the interaction promotes a response at molecular level. Another common application is the visualization of a presence of specific cell population, for example in inflammatory processes or presence of pathologically transformed tissues such as β -amyloid molecules in the brain in cases of Alzheimer's disease (Stuker et al., 2011). The highly attractive properties of the fluorescence imaging make it powerful tool for non-invasive investigation of biological systems in preclinical research and accordingly provoke remarkable efforts in the development and improvement of this field.

The imaging experiments described in the following work were performed with IVIS Spectrum CT System – optical imaging device for small animals in preclinical studies. It possesses advanced optical units such as ultra-sensitive CCD camera and full range excitation and emission filters which operate from visible to NIR light spectrum. IVIS provides bioluminescence and fluorescence imaging functionalities and 3D scanning mode which uses transillumination strategy. The generated 3D optical datasets paired with the system's X-ray CT and combined with the Living Image software for image analysis allows fluorescence detection and quantification in larger depths and in challenging cases where 2D imaging cannot provide sufficient solution (Tseng et al., 2015).

2.2. Bacterial ghost

Since decades the idea of a 'magic bullet' able to cure an active substance and recognise a given receptor excites the researchers. Development of advanced drug delivery systems owning the ability to reach precisely target site providing a therapeutic action should result in reduced serious toxic and noncurative side effects, decreased drug doses, improved pharmacokinetics and increased local drug concentration. The concept for perfect drug targeting vehicles assumes that it consists a therapeutic drug, a carrier of the drug molecules and a targeting moiety but the currently used approaches substitute the targeting moiety with physical targeting based on change of physical parameters, with passive targeting by natural patterns or simply with direct application of the drug. An alternative for active particle-based drug delivery system with very high potential are the bacterial ghosts (BGs) (Paukner et al., 2006).

Bacterial ghosts are empty envelopes of Gram-negative bacteria which have been produced by the controlled expression of lysis gene E of bacteriophage phiX174 and releasing all bacterial cytoplasmic content to the environment but preserving periplasmic components (Hajam, Dar, Won, & Lee, 2017; Langemann et al., 2010). Gene E codes a 91-aa membrane protein able to oligomerize and form a single transmembrane tunnel structure pervading the inner and outer membrane through which all nucleic acids, ribosomes and other constituents are expelled, resulting in an empty bacterial shell suitable for refilling with drugs, DNA or peptides. At the same time the cellular morphology remains similar to native bacteria and cell surface structures such as outer membrane proteins, lipopolysaccharides and peptidoglycans persist. The preservation of these envelope structures presumes that the antigen nature of the membrane components also remain intact and can elicit an immune response (Hajam et al., 2017; Lubitz, 2001). So far, several studies have been focused on revealing the E-lysis process, leading to the observation that the E-specific lysis tunnel formation is impossible to be accomplished in stationary phase host cells because it depends on mechanisms involved in cell division and in this regard the tunnel is located at division zones – the center or some of the poles of the bacteria. The following disposal of cytoplasmic substances is driven by the osmotic pressure difference between the surrounding environment and the cytoplasm. The mode of formation was first described as a three-phase process including a phase of integration of the polypeptide into the inner membrane with its hydrophobic N-terminal facing the periplasmic space and respectively the C-terminal in the direction of the cytoplasm, a second phase of conformational change during which the C-terminal domain shifts to the periplasmic space string along with oligomerization and third step of fusion of the inner and outer membrane evoked by exposure of the C-terminal domain of protein E to the surface of the host cell. The protein E-mediated lysis has been applied on several Gram-negative strains successfully deriving ghosts but not for Gram-positive bacteria. (Langemann et al., 2010; Schön, Schrot, Wanner, Lubitz, & Witte, 1995).

2.2.1. Bacterial ghosts as adjuvant particles

Owing to the combination of its unique properties, the BGs system can be used as a very specific delivery vehicle for medicaments and gene medicine or alone as an adjuvant. As it is mentioned above, the preserved pathogen-associated molecular patterns (PAMPs) and LPS have stimulatory effect on the immunocompetent cells such as monocytes, macrophages and dendritic cells (DCs) but also, they might have the ability to stimulate particular tumor cells in

direction of non-professional phagocytosing behavior. It is shown that melanoma cells are capable to act similar to antigen-presenting cells (APCs) and exposure to BGs results in raise in phagocytosis rate (Kudela, Juliana, & Lubitz, 2010). There are numerous of findings supporting the statement that BGs can be classified as potent immunostimulatory adjuvants. As most common example is pointed monophosphoryl lipid A derived from *Salmonella minnesota* that is known to interact with Toll-like receptor 4 a consequently supports the T-helper cells responses with induction of cytokines synthesis. Another role attributed to MPL is in increment of the migration and maturation of DCs (Riedmann, Kyd, Cripps, & Lubitz, 2007). TLRs are present on the adaptive immunity cells which is the main factor for the significant adjuvant potential of BGs. To the positive features of the BGs it's worth adding that the endotoxicity of the LPS does not prohibit the use of BGs as vaccine and even after intravenous administration of high doses of BGs in rabbits no toxic effect is indicated (H. J. Mader, Szostak, & Haslberger, 1997). Generally, BGs contribute to the stimulation not only to innate immune cells but also adaptive immune cells, efficiently inducing a potent immune response. A possible direction for future development and enhancing its potentialities is the expression of additional immunostimulatory molecules on their surface (Hajam et al., 2017).

2.2.2. Bacterial ghosts as carrier

As it is mentioned above, a selective drug delivery system with ability to target particular tissues is highly requisite with intention to raise significantly the efficiency of medical treatment, to decrease the required doses and last but not least to lower the severe side effects of the drugs (Huter et al., 1999). Thus, BG system represent a potential solution with broad spectrum of utility and possibilities for development. In the extended ghost system drugs, foreign proteins and nucleic acids can be immobilized within the BG in various ways – by tying up with the outer membrane, tethering to the inner membrane by specific anchor sequences or by exportation into the periplasmic space. The combination between the intact envelope structures able to bind to receptors on cell surfaces and the high loading capacity extremely extends ghost platform's capability to function as carriers and targeting systems. (Lubitz, 2001; Paukner et al., 2006). Depending on the bacteria strain that has been used for production of the ghosts and its individual surface characteristics, BGs have potential to be exploited for targeting broad range of body tissues and cells. Ever since the end of last century it has been started investigation of bioadhesive drug delivery systems based on bacteria's biorecognitive properties - a therapeutic agent has been linked to *E. coli* K99 fimbriae via a spacer, which

particularly clung to porcine intestinal enterocytes and also *Actinobacillus pleuropneumoniae* ghosts have been used in *in vivo* vaccination experiments on pigs for presentation of a potential drug carrier targeting the lung. Furthermore, the loading capability has been investigated by virtue of *E. coli* ghost that carry streptavidin captured to its membrane, so called streptavidin ghost which efficiently binds large biotinylated compounds. (Huter et al., 1999).

Perhaps one of the most significant application of the BGs is the delivery of chemotherapeutics. Since the anti-cancer drugs are highly cytotoxic agents, the benefits of them are diminished by the severe toxic side effects including cardiovascular damages. Most of these side effects are in result of non-specific targeting and high doses. Therefore, the role of BGs, as a non-toxic delivery system able to affiliate tumoricidal compounds without its modification and meanwhile capable to target particular cells of interest, can be considered as a significant and valuable achievement in cancer treatment (Kudela et al., 2010). As an example, for a model substance successfully loaded in BGs can be pointed out a study with the frequently used but highly cardiotoxic anticancer drug – doxorubicin (DOX). The cytotoxic compound has bound to the ghost's inner lumen nonspecifically with rate of approximately 9 weight DOX/weight BG. The DOX-loaded ghosts have been absorbed by colorectal adenocarcinoma cells (Caco-2), the drug has been released and subsequently accumulated in the nucleus of the cancer cells. In brief, the results show two magnitude of orders higher cytotoxicity for the DOX associated with ghosts in comparison to free DOX and in addition, the DOX-ghosts had noticeable antiproliferative effect at low DOX concentration, which had no effect on cell viability when applied as free DOX (Paukner, Kohl, & Lubitz, 2004). The reason why colorectal cancer is of great interest for the scientists is that this is one of the most common cancers worldwide and causes hundreds of thousands deaths per year. In most of the cases, the patients suffer from metastatic lesions and the first line treatment includes cytotoxic metal-based drugs such as cisplatin and oxaliplatin but drug resistance often occurs hampering the successes of the therapy (Mármol et al., 2017). The peritoneal carcinomatosis is the major cause of the high mortality rate of colorectal cancer which makes it an attractive target for improvement of the current strategy for treating this disease. It is known that the peritoneal cavity possesses high immune competence and this feature strongly affects the activity of oxaliplatin hence a combination of the drug with immunogenic adjuvants with ability to be specifically targeted has been further investigated. An experiment has been performed on mice injected with CT26 tumor cells and spread in the peritoneal cavity and thereafter treated with oxaliplatin, empty bacterial ghosts as a potent immune-stimulator or a combination of both. It is reported that the combination of the BGs and oxaliplatin resulted in decreased number of

lesions, activation of cellular immune response and significantly prolonged life span with comparison to the control groups (Groza et al., 2018). The mentioned results regarding targeted delivery of doxorubicin and oxaliplatin to colorectal tissues via BGs were supported and extended with a recent study that presents data about successful loading of another common drug - 5-Fluorouracil into *E. coli* BL21 bacterial ghosts, followed by slow dispense of the drug over an extended duration of time and subsequent delivery to colorectal adenocarcinoma cells with promising cytotoxicity activity (Youssof, Alanazi, Salem-bekhit, Shakeel, & Haq, 2019). These findings could be of great benefit to the patients because 5-FU is an agent that can be combined with variety of other cytostatic drugs for obtaining better effect and it is the major component of widely used clinical protocols for treatment of colorectal cancer such as FOLFOX and FOLFIRI because of its therapeutic advantages and generally mild side effects (R. M. Mader, Müller, & Steger, 1998).

The listed promising options that lie behind the exceptional BGs system non-surprisingly have aroused the interest of many research groups with aim is to investigate in details the biodistribution of the ghosts, the exact effects that they promote on the immune system, the impact of different ways of administration, new methods of improving the system etc.

2.3.Small interfering RNA technology

The discovery of the small interfering RNA (siRNA) and its ability to inhibit peculiar genes in many genetic diseases is one of the most important advances reached in gene regulation field and respectively, it is an attractive tool to study single genes or to develop potent therapeutics, especially against undruggable targets for example - for cancer treatment (Dana et al., 2017). Each siRNA molecule is capable to inactivate several RNA molecules in a sequence-specific manner which makes it the most promising type of RNA-based therapeutic oligonucleotide. However, numerous of chemical modifications of RNA have been required for modulation their activity and stabilization in biological fluids because of the relatively high molecular weight of the oligonucleotides and its hydrophilic nature. As a result, various siRNA-based drugs are undergoing clinical trials but still many unsolved problems remain and impede siRNA's full potential – it is lacking an effective means of delivering siRNAs to certain cell types and in addition, a risk of unwanted immune response presents (Chernikov, Vlassov, & Chernolovskaya, 2019). As the origin of most tumors are oncogenes or mutated tumor suppressor genes, cancer is one of the major targets of RNA interference-based therapy. A huge

advantage of this type of treatment is the ability to target multiple genes part of cellular pathways involved in tumor growth and it can be used to avoid multiple drugs' resistance and numerous side effects which are common results of chemotherapeutic overdose. Another benefit is the potential for development of personalized drugs for specific patients which are more potent and safer (Mansoori, Shotorbani, & Baradaran, 2014).

The delivery of nucleic acids such as siRNA has already become a core strategy for silencing unwanted gene expression and consequently suppressing tumor cell growth, even though a potent anticancer siRNA has a strong demand of an effective delivery system for proceeding to successful clinical application. Before reaching the cytoplasm of the target cell the siRNA complex should pass certain obstacles as avoiding kidney filtration, uptake by reticuloendothelial system which is composed of phagocytic cells or avoiding enzymatic degradation by nucleases in the plasma and tissues. In addition, the anionic and hydrophilic nature of the molecule prevents from crossing biological membranes which suggests that packaging vesicles or local administration strategies are needed in order to promote cellular uptake. The currently developed siRNA delivery systems that address the mentioned above problems include chemical modifications, lipid or polymer based carrier, conjugated siRNA delivery systems, co-delivery with anticancer drugs and nanoparticulate carrier (Singh, Trivedi, & Jain, 2018). As a local administration approach, it has been studied a pulmonary delivery method which may include inhalation, intranasal and intratracheal administration. The study demonstrates successful delivery to the lung and presents the dynamic biodistribution events by tracking fluorescently labelled siRNA (Geyer et al., 2017).

3. Aim of thesis

The present thesis is divided into two projects. The aim of the first part was to employ 3D fluorescence imaging tomography-based method to investigate *in vivo* biodistribution of bacterial ghosts labeled with near infrared emitting dye AlexaFluor750 and at the same time to optimize the process of analyzing of 3D optical datasets provided by the advanced optical imaging device - IVIS Spectrum CT System. The biodistribution studies include intraperitoneal administration of BG-AF750 in non-tumor bearing animals and in CT26 tumor bearing animals, followed by 3D FLIT in prone and supine position at different time points – 1 hour and 24 hours after the administration or after 2 hours, intending to investigate the preferable zones or organs of distribution and to localize BGs with respect to the tumor. The observations from the whole animal imaging were validated with organ imaging. For the optimization process different region of interest (ROI) sets were applied in combination of various threshold values and voxel minimum values with aim to develop a concrete pattern of analyzing and high-quality visual representation of 3D FLIT data.

The aim of the second project was to investigate dynamic biodistribution events after intratracheal application of siRNA labeled with AlexaFluor750 by combination of epifluorescence imaging and fluorescence imaging tomography. The animals were imaged in prone and supine position directly after the administration and after 24 hours, the observations were validated with organ imaging. A progress in pulmonary delivery of nucleic acids would greatly contribute to optimization of therapeutic concepts and establishment of possibility for direct treatment of lung diseases.

Additionally, an assessment of the Living Image software in the context of credible tool for biodistribution tracking *in vivo*, also falls within the scope of the study.

4. Material and Methods

4.1. Bacterial ghost project

4.1.1. BG project - animals, intraperitoneal administration, imaging

Balb/cJRj female mice (purchased from Janvier Labs, le Genest-Saint-Isle, France) were used for the Bacterial Ghost experiment. The imaging results analyzed in this thesis were obtained from animal experiments, were all animal procedures were approved by the local ethics committee and are in accordance with the Austrian law for the protection of animals and the EU directive 2010/63/EU.

All *in vivo* experiments mentioned below have been performed by Nadine Follrich. Detailed information about the animal care which includes housing under pathogen free conditions and feeding with autoclaved low Fluorescent diet is provided in Nadine's diploma thesis as well as the detailed information about the methods of shaving and imaging (Follrich, 2019).

The experimental animals are divided into two groups – tumor bearing and non-tumor bearing. 1×10^5 CT26^{F-luc} cells have been applied intraperitoneally to all tumor bearing mice and in addition Oxaliplatin has been injected intraperitoneally at 6mg/kg. Both groups have been injected intraperitoneally with AF750 labelled Bacterial ghosts with dosage of 4×10^8 BGs in 250 μ l of HBG per mouse and the used Buffer has been 5% Glucose (B.Braun, Melsungen AG, Germany) at the same dose. As contrast agent for all animals Gastrografin (Bayer) was used, 15ml from which have been added in 200 ml of water overnight to the water bottles. As anesthetic agent, Isoflurane (Rothacher Medical GmbH, Switzerland) was used at – 5% as initial dose and 2% for maintaining the desired anesthetic depth. For eyes protection has been used eye ointment (VitA POS®, Ursapharm, Saarbrücken, Germany).

For organ imaging control mice have been used, whereas the 3D FLIT imaging has been performed only on one animal per round because of the technical characteristics of the device

Images were acquired using the IVIS Spectrum CT System and were analyzed using Living Image 4.5.1 software (Perkin Elmer Inc., Waltham, MA).

Mouse ID	Control mouse ID	Treatment	Procedures
Non-tumor bearing animals			
<i>3D FLIT after 2 hours</i>			
MCT-0267 MCT-0268	MCT-0270	Intraperitoneal injection of 4×10^8 AF750 labelled Bacterial ghosts Oral administration of Gastrografin Intraperitoneal injection of 300 μ l Iopamidol (120 μ l Iopamidol/180 μ l 5% glucose)	*0h – Intraperitoneal injection of Bacterial ghosts Followed by: Iso anesthesia Eye ointment Shaving Body weighting Intraperitoneal injection of Iopamidol Fixation with non-reflection black tape on IVIS platform 2D FLI 2h – 3D FLIT , supine, Stage: B, Transillumination points 12, CT Medium resolution. Followed by: Deep iso anesthesia Cervical dislocation <i>Ex vivo</i> imaging 5h – Organ imaging
<i>3D FLIT after 1 hour and after 24 hours</i>			
MCT-0275 MCT-0276	MCT-0277	Intraperitoneal injection of 4×10^8 AF750 labelled Bacterial ghosts Oral administration of Gastrografin	0h – Intraperitoneal injection of Bacterial ghosts Followed by: Iso anesthesia Eye ointment Shaving Body weighting Intraperitoneal injection of Iopamidol

		Intraperitoneal injection of 300µl diluted Iopamidol (120µl Iopamidol +180µl 5% glucose)	<p>Fixation with non-reflection black tape on IVIS platform</p> <p>2D FLI</p> <p>1h – 3D FLIT, supine/prone, Stage: B, Transillumination points 12, CT Medium resolution</p> <p>24h – 3D FLIT supine/prone</p> <p>Followed by:</p> <p>Deep iso anesthesia</p> <p>Cervical dislocation</p> <p><i>Ex vivo</i> imaging</p> <p>Organ imaging</p>
Tumor bearing animals			
<i>3D FLIT after 1 hour and after 24 hours</i>			
MCT-0271	MCT-0266	Intraperitoneal injection of 1x10 ⁵	<p>Procedures before the administration of BGs:</p> <p>Iso anesthesia</p> <p>Shaving</p> <p>Ear punching</p> <p>Tail marking</p> <p>Intraperitoneal injection of CT26^{F-Luc}</p> <p>Body weighting</p> <p>Fixation with non-reflecting black tape on IVIS platform</p> <p>2D BLI</p> <p>Two intraperitoneal injections of Oxaliplatin</p> <p>Subcutaneous injection of D-Luc</p> <p>0h – Intraperitoneal injection of Bacterial ghosts</p> <p>2D BLI</p>
MCT-0272		CT26 ^{F-Luc} tumor cells	
MCT-0273	MCT-0274	Subcutaneous injection of D-Luc	
MCT-0278		6mg/kg Oxaliplatin	
MCT-0279		Intraperitoneal injection of 4x10 ⁸ AF750 labelled Bacterial ghosts	
MCT-0280	MCT-0265	Oral administration of Gastrografin	
		Intraperitoneal injection of 300µl	

		Iopamidol (120µl Iopamidol/180µl 5% glucose)	1h – 3D FLIT (only for MCT-0280), supine, Stage: B, Transillumination points 12, CT Medium resolution 24h – 3D FLIT prone (supine for MCT- 0280, prone and supine for MCT-0279), Stage: B, Transillumination points 12, CT Medium resolution. Followed by: Deep iso anesthesia Cervical dislocation <i>Ex vivo</i> imaging Organ imaging
--	--	--	--

* The time points included in the table are intended to indicate only the intervals between the administration of Bacterial ghosts and the moment of imaging. They do not present the full timetable of the performed procedures. Some of the procedures such as shaving, anesthesia and others are performed more than once.

4.1.2. BG project – data analysis

The process of analysis of the BG data, obtained from the FLIT, includes measurement of the total radiant efficiency in three main areas – thoracic, abdominal and pelvic on which were drawn ROIs with approximately similar shape and size for each animal. For more detailed evaluation and assessment of the software’s impact on the results, two more mandatory ROIs were applied – one around the whole body of the experimental animal and a background ROI with the same dimension as the whole-body ROI but positioned beyond the outline of the test object with aim to be used as control and to ensure the lack of false signal generated by the software.. The values detected within these two ROIs are used for monitoring the changes in the total concentration of the fluorophore at the chosen time points and for normalization of the data with regard to potential background noise. The size and the shape of the background ROIs are identical to the ROIs drawn around the body of the respective mouse because they are generated simply by copying of the whole-body ROI. The detected background noise is compared to the detected body signals and presented in the table below:

Image:	Total value – Background ROI:	Total value – Whole body ROI:
MCT-0267 2h supine	4,19E+04	1,06E+07
MCT-0268 2h supine	4,11E+04	9,81E+06
MCT-0275 1h prone	1,82E+04	1,16E+07
MCT-0275 24h prone	1,45E+04	1,00E+07
MCT-0275 1h supine	3,09E+04	1,08E+07
MCT-0275 24h supine	1,70E+04	9,73E+06
MCT-0276 1h prone	2,56E+04	1,11E+07
MCT-0276 24h prone	1,19E+04	9,87E+06
MCT-0276 1h supine	1,54E+04	1,02E+07
MCT-0276 24h supine	1,67E+04	9,88E+06
MCT-0280 1h supine	1,78E+04	9,50E+06
MCT-0280 24h supine	1,39E+04	9,39E+06
MCT-0271 24h prone	1,96E+04	1,11E+07
MCT-0272 24h prone	2,80E+04	1,04E+07
MCT-0273 24h prone	3,34E+04	9,95E+06
MCT-0278 24h prone	1,43E+04	1,15E+07
MCT-0279 24h prone	2,51E+04	1,07E+07
MCT-0279 24h supine	2,38E+04	9,11E+06

The ROIs sets applied on images in prone position slightly differ from the sets applied for supine position because of the specifics such as body size, shape and shooting angle. ROIs with different sizes and locations also were applied on every zone where strong signal were noticed and the total source intensity were measured as well, accompanied by organ identification in the cases where it was possible. The tools provided by the software, such as voxel minimum change, threshold increase and application of a surface mode, were used for better visualization, reduction of the background noises and refinement of signal localization. The observations were validated by organ imaging.

4.2. siRNA project

4.2.1. siRNA project – animals, intratracheal administration, imaging

Balb/cJRj female mice (purchased from Janvier Labs, le Genest-Saint-Isle, France) were used for the siRNA experiment. The imaging results analyzed in this thesis were obtained

from animal experiments, were all animal procedures were approved by the local ethics committee and are in accordance with the Austrian law for the protection of animals and the EU directive 2010/63/EU. All *in vivo* experiments involved in the siRNA project have been performed by Antonia Geyer. The animals were housing under pathogen free conditions. Autoclaved water and food (standard rodent diet; SSniff, Soest, Germany) were provided ad libitum. Food supply was switched to a low fluorescent diet (BROGAARDEN D10001 AIN-76A; Korn & Foderstoffer ApS, 3540 Lyngø, Denmark) (Geyer et al., 2017).

AF750 labeled siRNA polyplexes have been delivered intratracheally to two experimental animals – MCT-0209 and MCT-0215. The polyplexes have been prepared by mixing LPEI (linear polyethylenimine, 10kDa) with AF750-siRNA at two different N/P ratios- 6 and 10. Mouse MCT-0209 has been administered with N/P6 AF750-siRNA polyplexes and mouse MCT-0215 has been administered with N/P10 AF750-siRNA polyplexes, above the tracheal bifurcation to ensure direct delivery into both lungs.

Both mice were imaged by IVIS Spectrum CT in prone and supine position. 2D fluorescence imaging was performed in the epifluorescence mode with automated exposure time, excitation filter BP 745/30nm and emission filter BP 800/20 nm immediately after the administration and 24 hours later. At the same time points 3D FLIT measurement was performed, mice first underwent a CT scan (low resolution setting) followed by fluorescence imaging in the transillumination mode.

4.2.2. siRNA project – data analysis

The process of analysis of the siRNA, obtained from the 2D epifluorescence imaging, includes measurement of the total radiant efficiency in two concrete regions of interest where signal was visually identified – kidney area and lung area. For both mice, in both positions – prone and supine and at both time points – 0h and 24h, the ROIs were completely identical regarding shape and size for a proper comparison, but the exact positions were slightly adjusted according to the location of the organs. ROIs were not applied in the absence of a convincing visual signal, even assuming that an organ is not correctly detected, inasmuch as this experiment is a pilot one and aims establishment of an impartial model for analysing further experiments of this particular study. The used settings are image adjustments – changing the minimum of the colour scale, the smoothing and the binning. At the FLIT analyzing, as well as at the 2D, the applied set of ROIs is identical for both animals, in both positions and at both time points but some additional ROIs were included. Besides the two kidney ROIs and the lung ROI, also a whole-body ROI was used for evaluating the total fluorescence and a control ROI

were drawn beyond the outline of the body to assess the impact of software background. The detected background noise is compared to the detected body signals and presented in the table below:

Image:	Total value – Background ROI:	Total value – Whole body ROI:
MCT-0209 0h prone	2,61E+04	3,35E+06
MCT-0209 24h prone	2,23E+04	3,45E +06
MCT-0209 0h supine	2,39E+04	3,20E+06
MCT-0209 24h supine	2,44E+04	3,46E+06
MCT-0215 0h prone	2,36E+04	3,01E+06
MCT-0215 24h prone	1,75E+04	3,35E+06
MCT-0215 0h supine	2,30E+04	2,96E+06
MCT-0215 24h supine	2,18E+04	3,20E+06

The used setting tools coincide with those used in the BGs project - changed voxel minimum, increased threshold and applied surface mode, aiming better visualization, deprivation of the background noises and refinement of signal localization. The observations were validated by organ imaging.

5. Results and Discussion

5.1. Bacterial Ghost biodistribution

The bacterial ghosts' biodistribution was investigated with experiments on 10 different mice – 6 tumor bearing and 4 tumor free animals, excluding the reference mice. The non-tumor bearing group is subdivided into two small groups – two animals were imaged 2 hours after the intraperitoneal injection and the other two were imaged after 1 hour and after 24 hours. On every image a set of 5 mandatory ROIs were applied – whole body, control with the shape and the size of the whole-body ROI, thoracic area, abdominal area and pelvic area and the total radiant efficiency were measured and evaluated. In addition, signal evaluation was done on every zone visualized as signal positive. Due to the anatomical specifications, the three main areas – thoracic, abdominal and pelvic, cannot be precisely equated, therefore, the comparison is made on the basis of a clear signal.

5.1.1. Bacterial ghost biodistribution in non-tumor mice – 2 hours after administration

The non-tumor bearing mice were injected intraperitoneally with bacterial ghosts labeled with AlexaFluor750. Two hours after the administration the animals were imaged in supine position (Fig.4). Five hours after the intraperitoneal injection, the mice were sacrificed under anesthesia by cervical dislocation. Afterwards the organs were taken out and imaged for organ validation (Fig.6).

The visual representation of the results from the imaging after 2 hours displays distinct signals in the liver and the gastrointestinal tract for the first mouse and in the zone around the uterus fat for the second mouse (Fig.4). It is possible the origin of the single detected intense signal in mouse MCT-0268 to be the position of the injection, since the imaging is performed shortly after the administration. Also, it is taken into account that a more superficial signal, that would be caused by an intraperitoneal delivery, is more likely to be reflected, despite the supposed capability for deeper penetration of the 3D imaging method. ROIs were drawn around the fluorescent areas and the total value were estimated but a direct comparison on this criterion between the two animals was not justified. However, the total values from measurement show approximately equal distribution by areas for both animals (Fig.5). The total values detected into the whole body ROIs are $1,06E+07$ for MCT-0267 and $9,77E+06$ for MCT-0268, this data is normalized by extracting the negligible signal disclosed as software background measured

in the control ROIs– respectively $4,19E+04$ and $4,11E+04$, as it is pointed out in the section “Materials and methods”. It is also observed that the difference between the areas is not so significant, which leads to the assumption that the biggest part of the imaged signal cannot be visualized by the software at least in the particular case. Anyway, the high values in the abdomens can be admitted as a sign that after two hours the bacterial ghosts are already distributed in most of the organs, especially in the gastrointestinal tract.

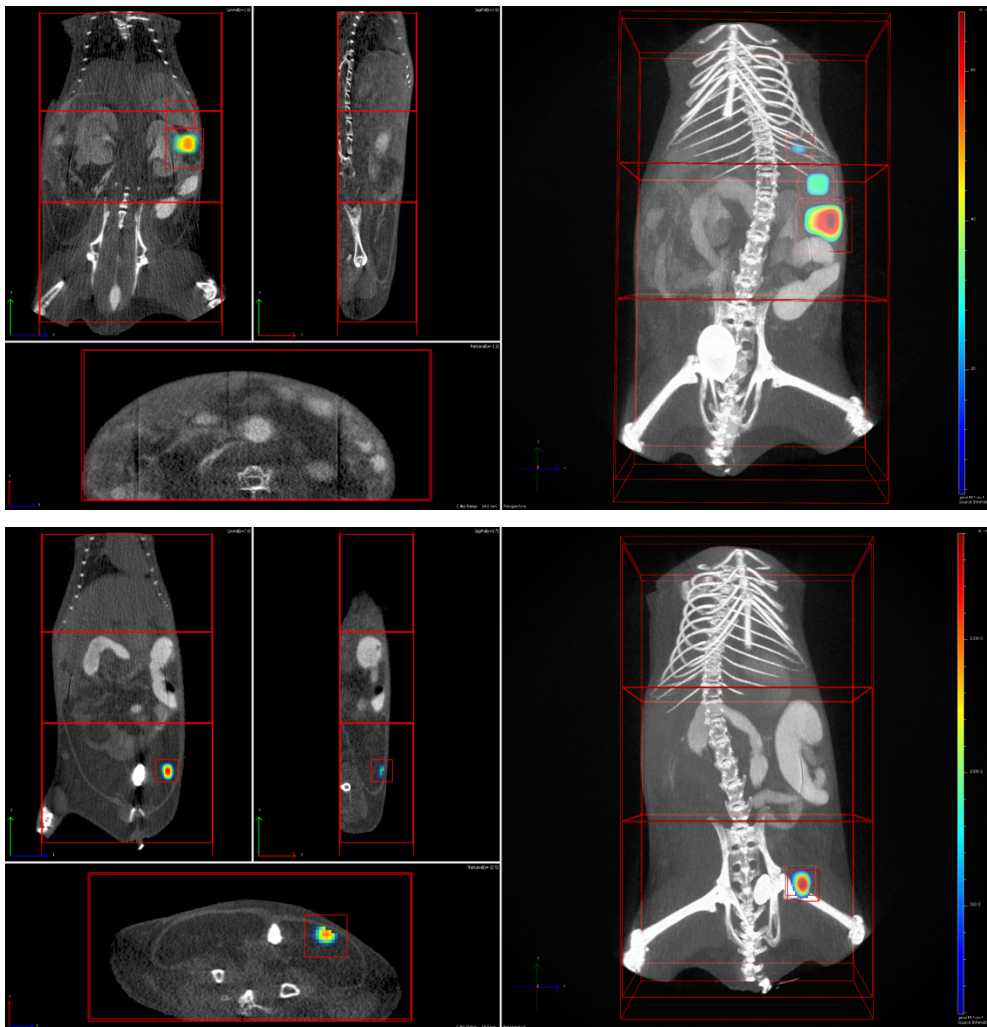


Fig.4. 3D fluorescent imaging performed 2 hours after the intraperitoneal injection of the AF750 labeled bacterial ghosts to two non-tumor mice - MCT-0267(top panel) and MCT-0268 (lower panel) imaged in supine position with applied ROI sets. Settings adjustments: Threshold top panel - increased to $1.90e1$, voxel minimum – 3.40 . Threshold lower panel - increased to $2.28e2$, voxel minimum – $9.50e1$.

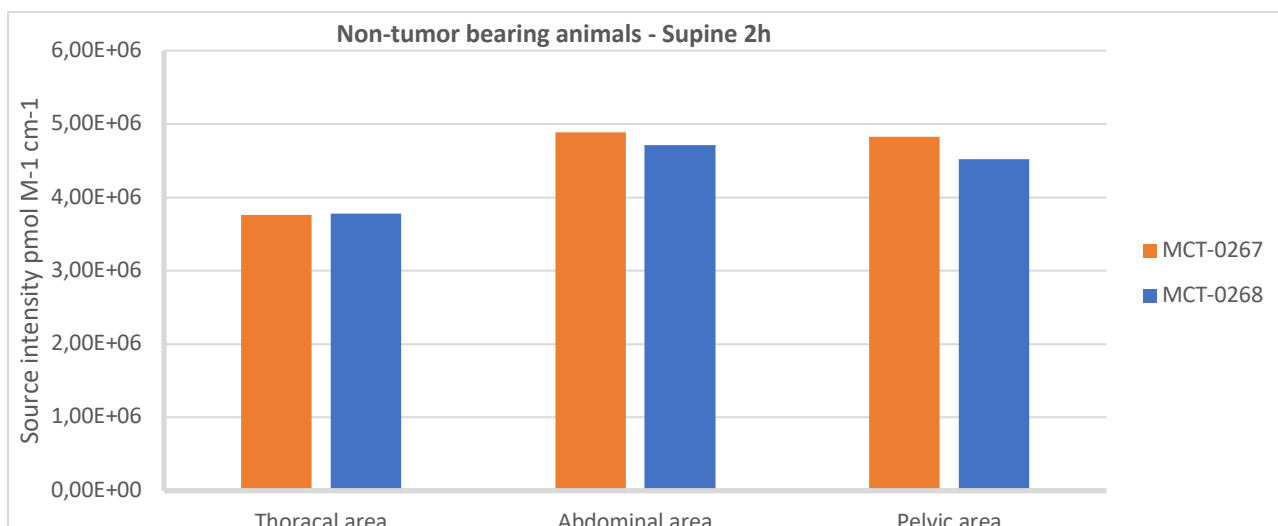


Fig.5. Graphical representation of the total values measured in the thoracal, abdominal and pelvic areas of MCT-0267 and MCT-0268 2 hours after intraperitoneal injection of the AF750 labeled bacterial ghosts and measured in supine position.

Five hours after the injection, the mice were sacrificed under anaesthesia by cervical dislocation. For validation of the observations made during the FLIT analysis, the organs were carefully removed and imaged. The organ validation shows that in five hours BGs are able to reach widespread distribution across all major organs (Fig.6). Unlike what is displayed on the 3D image, the organ image reveals signal everywhere. This can be easily explained by the lack of overcoming of the surrounding tissues, which make it difficult to detect a deeper positioned signal, as in whole body imaging. However, partial confirmation of the visual results was obtained with respect to the organs with highest signal. On the other hand, the measured total values in the three main areas (Fig.5) which indicate for almost equal distribution in the thorax, abdomens and pelvic, could be considered validated by the organ measurements (Fig.7) since the organs with highest fluorescence are situated at various locations within the body.

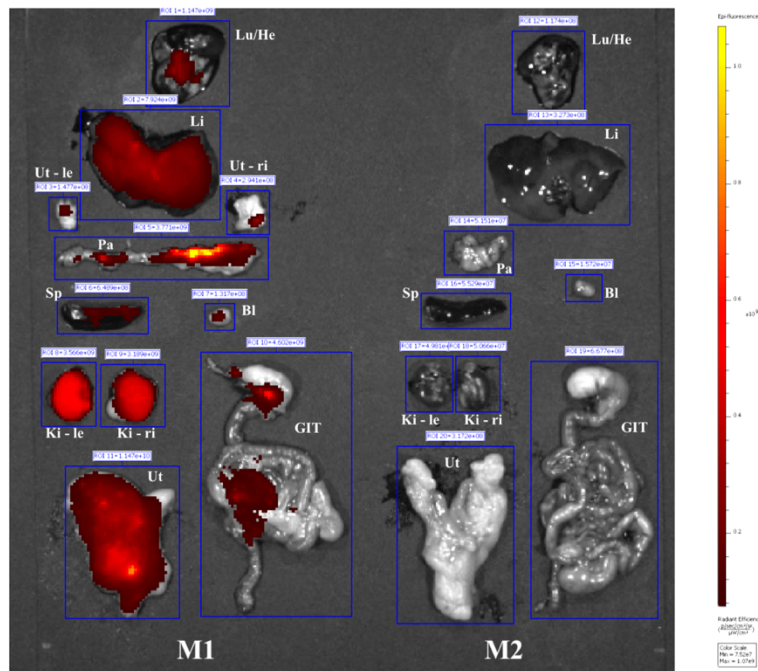


Fig. 6. 2D fluorescence organ imaging five hours after the intraperitoneal injection of AF750 labeled bacterial ghosts. The organs of the non-tumor bearing mouse (M1: MCT-0267) are shown on the left side and the organs of the reference mouse (M2: MCT-0270) are on the right side. The threshold is based on the referent animal. Labels legend: Lu/He = Lung/Heart, Li = Liver, Ut - le/ri = Uterus fat left/right, Pa = Pancreas, Sp = Spleen, Bl = Bladder, Ki - le/ri = Kidney left/right, Ut = Uterus, GIT = Gastrointestinal tract.

The chart displays a significant presence of bacterial ghosts in the uterus of both animals five hours after intraperitoneal administration (Fig. 7). Considerable are also the signals measured in the liver, the pancreas, the kidney and the gastrointestinal tract. The measured values fully match to the visual representation (Fig. 5).

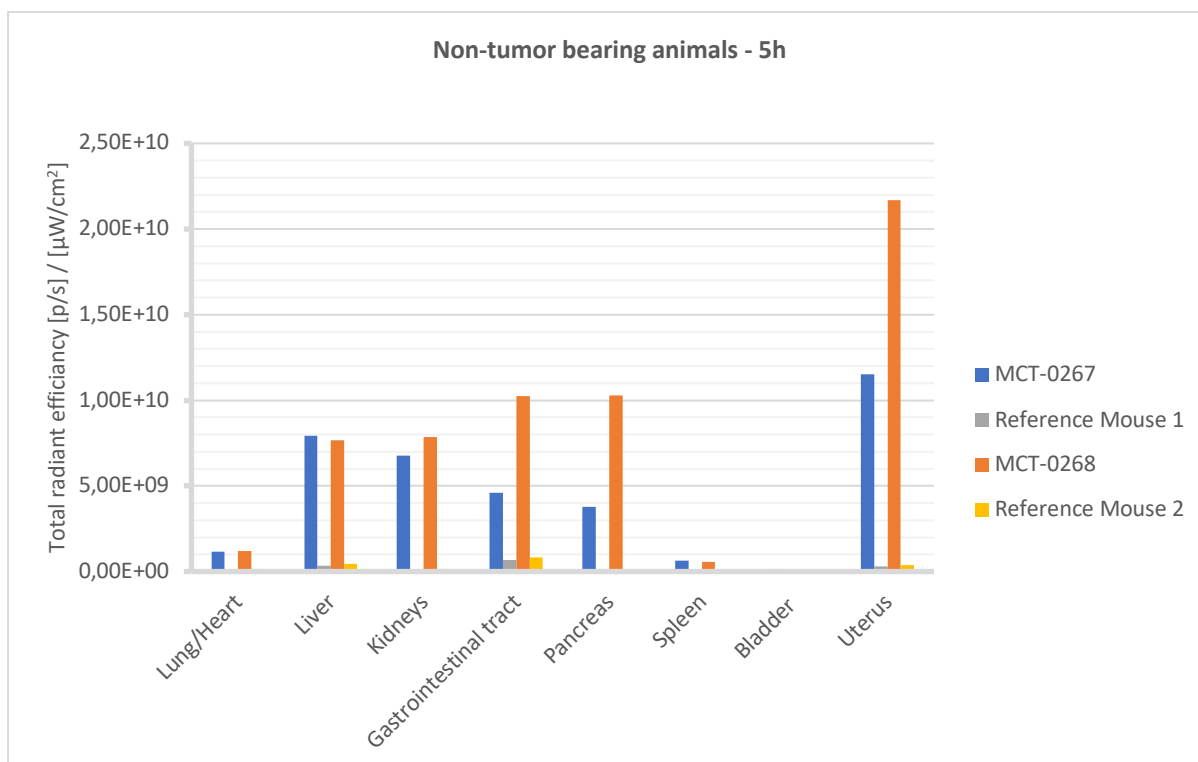


Fig.7. Graphical representation of the average intensity of the organs of mice MCT-0267 and MCT-0268 and the reference mouse MCT-0270 are shown. The imaging was done five hours after the administration of BG-AF750.

It could be summarized that the presented round of analysis leads to two main observations. First is based on the considerably high total radiant efficiency measure after only 5 hours in organs involved in the metabolism, such as liver and kidney. This suggests a relatively rapid spread of the BGs. The second and most substantial observation is that the BGs show significantly high preference to the uterus area.

5.1.2. Bacterial ghost biodistribution in non-tumor mice – 1 hour and 24 hours after administration

Another two non-tumor bearing mice were injected intraperitoneally with bacterial ghosts labeled with AlexaFluor750 for further investigation of the biodistribution after different time intervals. One hours after the administration the animals were imaged in both prone and supine position. Twenty-four hours after the intraperitoneal injection, the mice were imaged again and immediately after that they were sacrificed under anesthesia by cervical dislocation. Afterwards the organs were taken out and imaged for organ validation.

The visual representation of the results from the imaging after 1 hour displays BGs distribution in various parts of the gastrointestinal tract (Fig.8 left, Fig.9 left) and this applies for both animals in both prone and supine position. The average of the signals measured into

the gastrointestinal tract at all four images after 1 hour is $4.77E+05$ - a remarkably high number for such small ROIs with comparison to the average of the whole-body ROIs which is $1,09E+07$. Strong signals are observed also in the pancreas, the spleen and part of the liver of both mice although is detected only in prone or supine position and it is not visible from both imaged sides. Evidently, the BGs are distinguished by fast biodistribution and can provide the valuable benefit of quick access to hardly reachable organs which are from very high interest as stomach, intestines and pancreas.

The visual representation of the results from the imaging after 24 hours of mice MCT-0275 and MCT-0276 in prone (Fig.8 right, Fig.9 right) and supine position displays high concentration of BGs into the pancreas. The average of the signals measured into the pancreases of both animals at both positions is $1,63E+05$. The average of whole-bodies ROIs is $9,86E+06$. The other region highly preferred by the labeled ghosts is the one around the uterus which may include also the uterus fat. The reliability of the signals in this area after only 1 hour is doubtful and it could be supposed to be a result of proximity to the injection side which is known to be near by the pelvis. However, the results of this round of the experiment demonstrate significant concentration of BGs into the uterus' tissues and the fat around it long time after the administration.

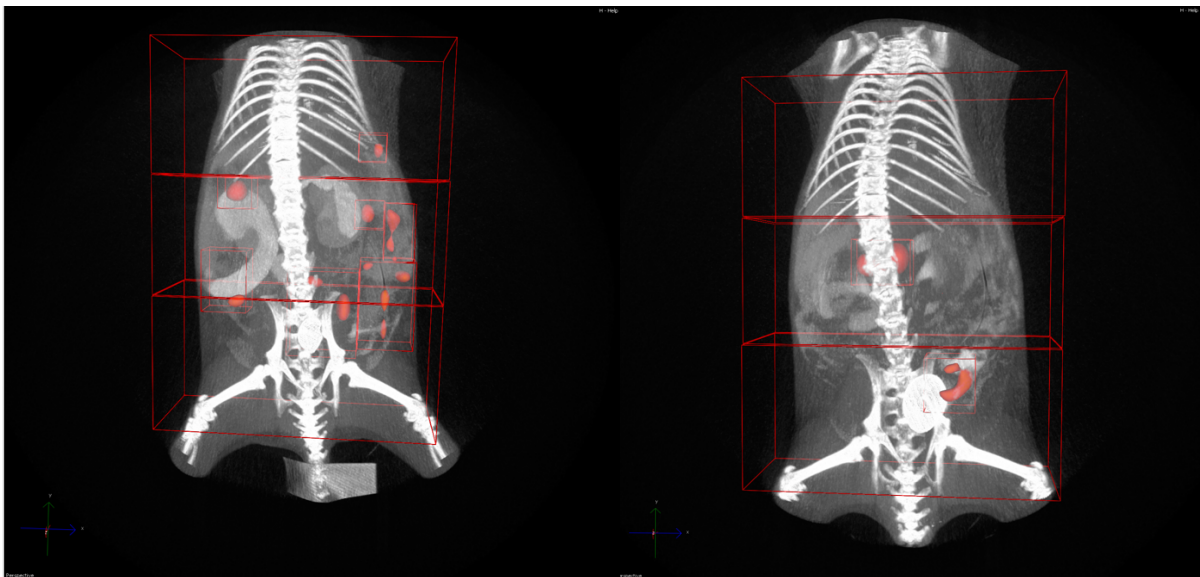


Fig. 8. 3D fluorescent imaging performed 1 hour (left image) and 24 hours (right image) after the intraperitoneal injection of the AF750 labeled bacterial ghosts to the treated non-tumor mouse MCT-0275 imaged in prone position with applied ROIs sets. Settings adjustments: surface mode, threshold left image – $8.19e-8$, voxel minimum left image - $3.89e2$, threshold right image - $7.55e-7$, voxel minimum right image - $1.70e2$.

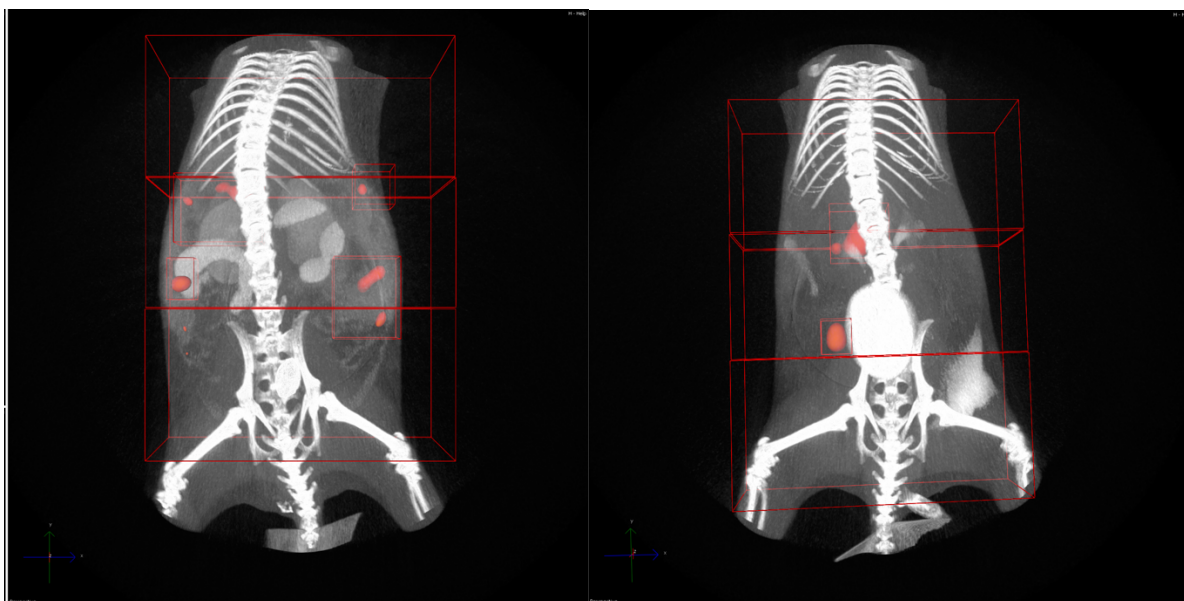


Fig.9. 3D fluorescent imaging performed 1 hour (left image) and 24 hours (right image) after the intraperitoneal injection of the AF750 labeled bacterial ghosts to the treated non-tumor mouse MCT-0276 imaged in prone position with applied ROIs sets. Setting adjustments: surface mode, threshold left image – $1.36e-5$, voxel minimum left image - $4.47e2$, threshold right image - $2.60e-2$, voxel minimum right image - $1.90e2$.

The 3D visualization is confirmed by the total value measurements (Fig.10) – shortly after the administration of the formulation, noticeably high is the signal in the abdominal area then decreases at the expense of the pelvic area where the uterus is placed. The non-negligible columns illustrating the area around the thorax presumably reflects the detected liver signal (Fig.8, Fig.9) and the very strong fluorescence coming from the pancreas which may partially engage the thoracic area, depending on the position of the mouse during the imaging. During the process of analyzation, the total values were measured before and after the threshold and the voxel minimum adjustments. This was done in order to crosscheck whether the capabilities of the software for fluorescent signal detection could be affected by the surface settings. The results showed that the accuracy of the data is not tarnished by the application of the tools for better visualization and the threshold adjustments.

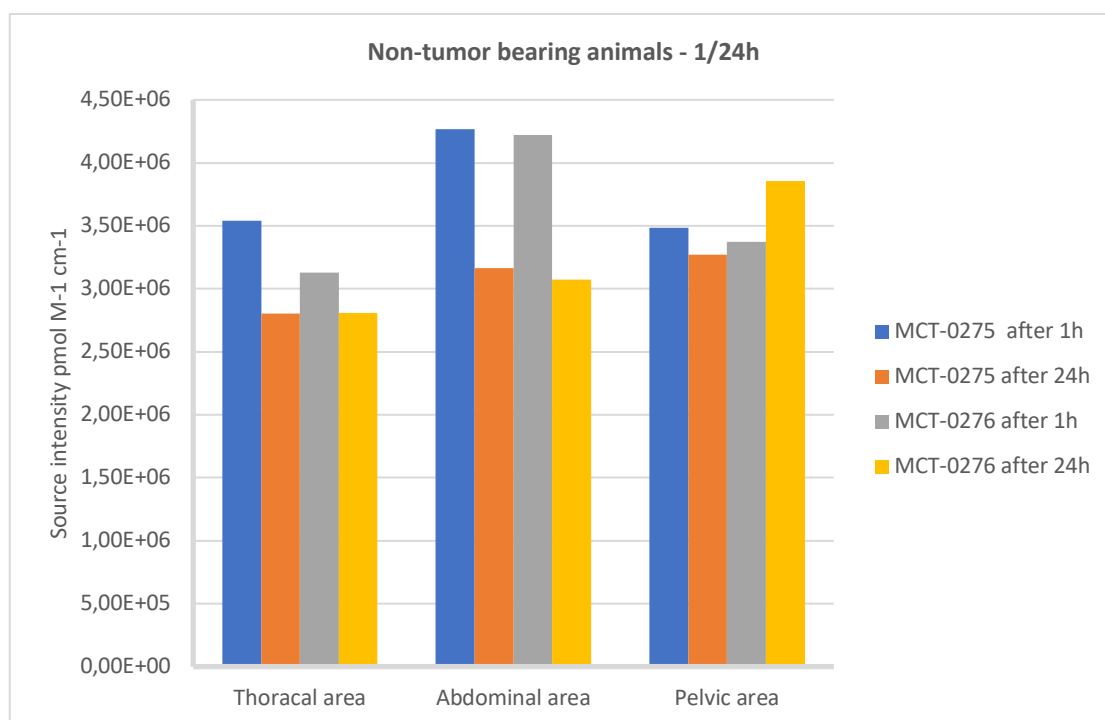


Fig.10. Graphical representation of the total values measured in the thoracal, abdominal and pelvic areas of MCT-0275 and MCT-0276 1 hour and 24 hours after intraperitoneal injection of the AF750 labeled bacterial ghosts.

Twenty-four hours after the injection, the mice were sacrificed under anaesthesia by cervical dislocation. For validation of the observations made during the FLIT analysis, the organs were carefully removed and imaged. The 2D organ imaging (Fig.11) confirms the 3D FLIT imaging observations made 24 hours after the administration of the formulation – high signals were detected in the pancreas and the uterus, further signals with significantly less intensity were detected in small areas of the lung, the liver and the uterus fat. A comparison between the organ validation from the previously discussed round which was performed 5 hours after the injection (Fig. 6.) and the currently discussed validation 24 hours after the administration of BG-AF750 (Fig.11.) indicates for widespread distribution of the fluorescent labeled ghosts in the first hours after the administration which may explain the excellent immunostimulatory properties of the bacterial ghosts with its pervasive circulation and consequently fast interaction with the immune cells. On the other hand, one day later the concentration in the whole body remains nearly the same with very slight negligible decrease – average of the values after 1 hour is 1.09E+07 and 9.85E+06 after 24 hours, but the detected signals are almost precisely concentrated in certain organs – uterus and pancreas. The graphical representation of the total radiant efficiency measurements (Fig.12) affirm the visualization

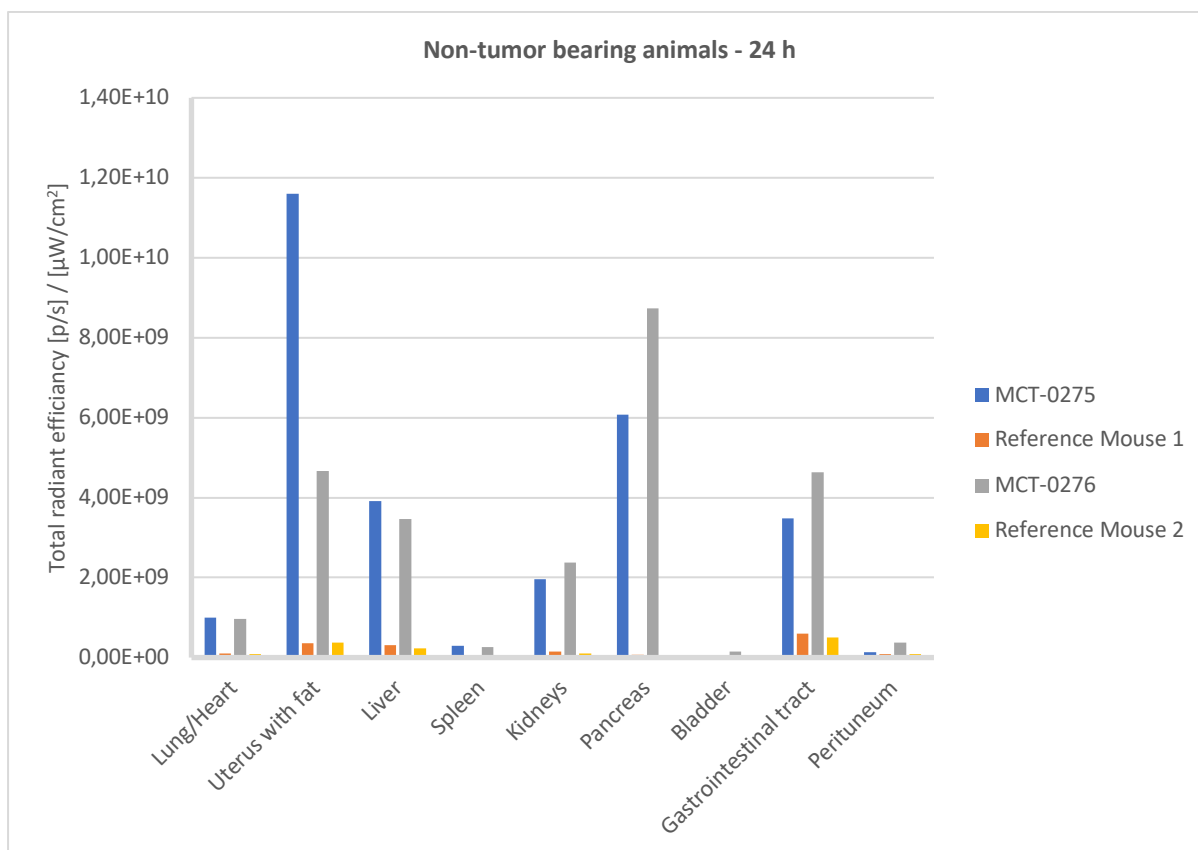


Fig.12. Graphical representation of the average intensity of the organs of mice MCT-0275 and MCT-0276 and the reference mouse MCT-0277 are shown. The imaging was done twenty-four hours after the administration of BG-AF750.

The conclusion that can be drawn after this round of the experiment that focuses on non-tumor bearing mice, confirms the observation on the rapid and extensive distribution of the BGs immediately after the intraperitoneal injection with considerable preference for organs in the gastric cavity, and in particular for the intestines. The total amount of the ghosts detected in the bodies of the animals 24h after the administration remains almost unchanged with comparison to the measurements made after 1 hour but the two time points differ in the locations with higher concentration – after 24 hours BGs distinctly target the pancreas and the uterus.

5.1.3. Bacterial ghost biodistribution in tumor bearing mice (24h after administration)

For the study of biodistribution of bacterial ghosts in tumor bearing animals a total of nine animals were used, three of which were used as reference mice for organ validation. The procedures performed on the six experimental animals include intraperitoneal injection of CT-26F-luc tumor cells on the first day, followed by intraperitoneal injection of 6mg/kg oxaliplatin three and six days later, Gastrografin – seven days later and intraperitoneal injection of AF750

labeled bacterial ghosts eight days after the CT-26F-luc administration (Follrich, 2019). Twenty-four hours after the administration of the BG formulation, five of all six animals underwent 3D FLIT imaging in prone position and instantly afterwards they were sacrificed under anesthesia by cervical dislocation and the organs were taken out and imaged for organ validation. Animal MCT-0280 were image in supine position 1 hour and 24 hours after the BG-AF750 injection, the organ validation protocol was the same.

The visual representation of the results from the imaging of MCT-0279 after 24 hours (Fig.13, Fig.14), displays BGs distribution in part of the gastrointestinal tract and this applies for most animals tested in this round. The visualized signal in the tumor bearing animals is heterogenous and covers large number of organs of which liver, kidney, uterus fat and lungs were identified. However, there is a clear tendency for ghosts to spread in the gut and the area around the uterus. In some cases, the strength and proximity of the detected fluorescence interfere with the precise determination of the organ, especially when it comes to the stomach cavity. Accordingly, the observed results of the 3D imaging suggest that some of the identified signals could interflow with the one from the pancreatic zone. These assumptions are made on the basis of all images from this round, Fig.13 and 14 are examples presenting only animal MCT-0279. Figure 14 represents the surface mode – a useful tool provided by the software for optimal 3D visualization of the detected signals.

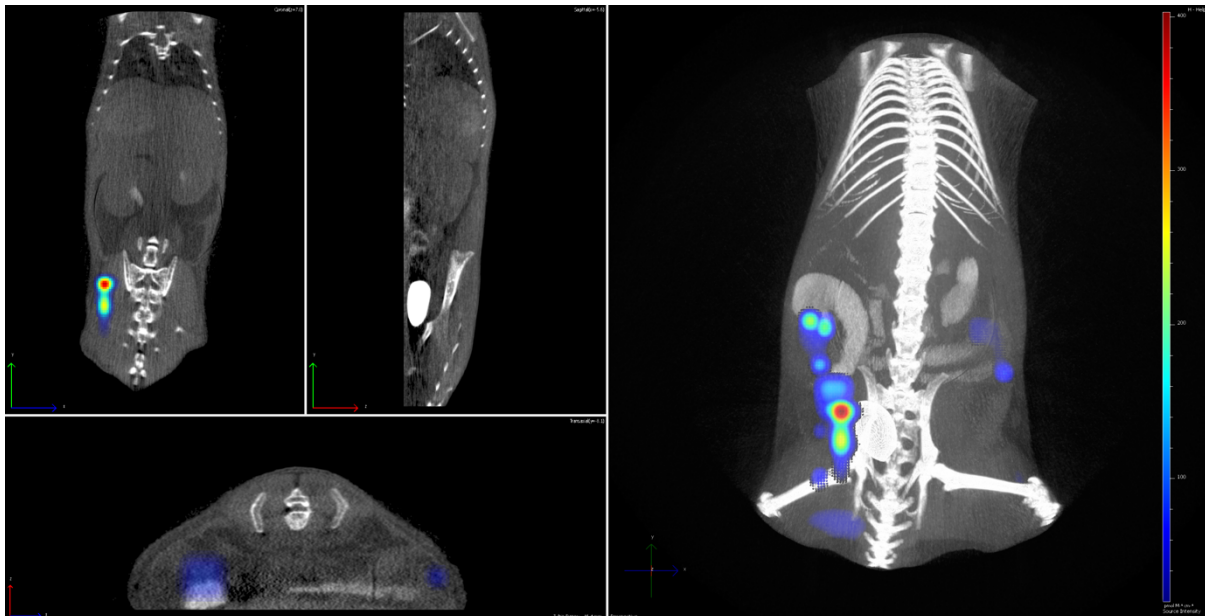


Fig.13. 3D fluorescent imaging performed 24 hours after the intraperitoneal injection of the AF750 labeled bacterial ghosts. The images display the treated tumor bearing mouse MCT-0279 in prone position in the original view provided by Living Image 4.5.1 software. The threshold and the voxel minimum remain unchanged according to the original settings, respectively – $2.90e-7$ and $2.02e1$.

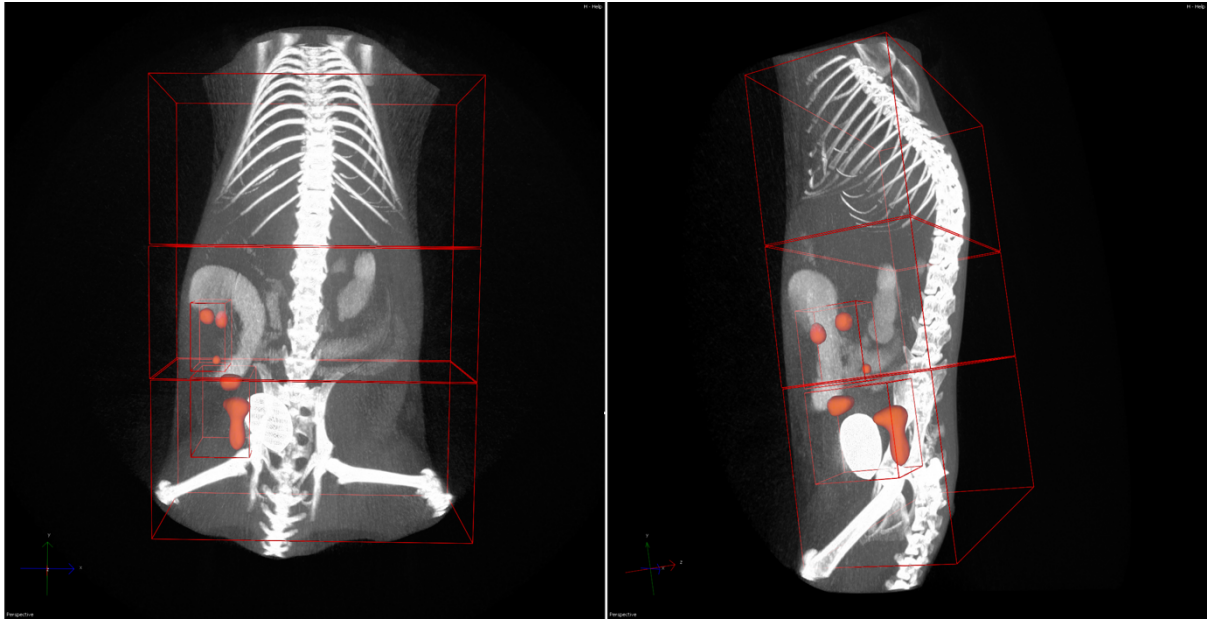


Fig.14. 3D fluorescent imaging performed 24 hours after the intraperitoneal injection of the AF750 labeled bacterial ghosts on the treated tumor bearing mouse MCT-0279 imaged in prone position with applied ROIs sets. For optimal 3D visualization is used surface mode provided by the software. The threshold for the images is according to the original settings – $2.90e-7$, the voxel minimum is set to $1.13e2$.

The analysis of the average values measured in the three conditionally determined zones – thorax, abdomens and pelvis, reveals highest concentration of BGs in the pelvic area (Fig.15). Nevertheless, the difference between the three columns is insignificant and the values are too close to make a firm conclusion based only on the 3D imaging in this round of the experiment. There is also a contradiction between the general graph (Fig.15), with a focus on the low signal measured in the abdominal area and the information that comes from the 3D visualization (Fig.13) where the gastrointestinal tract is massively identified as BG positive.

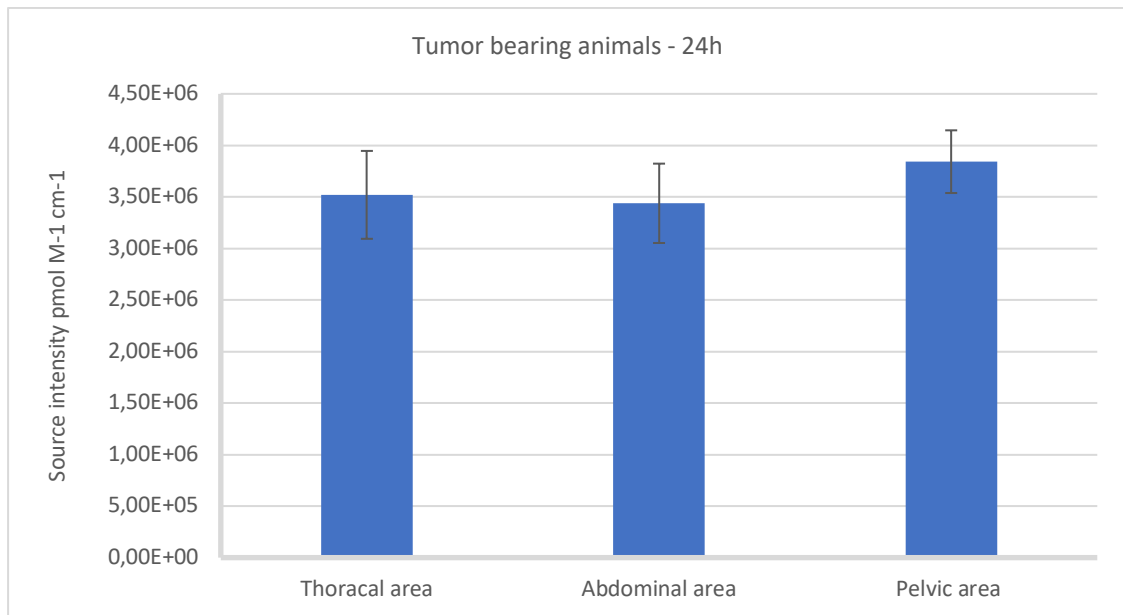


Fig.15. Graphical representation of the average total value measured in the thoracal, abdominal and pelvic areas of MCT-0271, MCT-0272, MCT-0273, MCT-0278 and MCT-0279 24 hours after intraperitoneal injection of the AF750 labeled bacterial ghosts and measured in supine position.

For further investigation and broadening the spectrum of observations, one of the animals – MCT-0280 was imaged in supine position at two time points – one hour after the administration of the labeled BGs and twenty-four hours after the administration (Fig.16). A specific signal was detected out of the pre-selected areas, one hour after the administration. The signal is located beneath the pelvic area, very close to the tail and after careful consideration, it was found that it most likely came from the injection location. Despite the high concentration of the BGs at the administration site, once again rapid spread in the gastrointestinal tract is observed. Another recurring important feature is the almost unchanged amount of detected BGs in the body 1 hour and 24 hours after the administration –the total values are respectively 9.48E+6 and 9.38E+6. The graphical representation of the total values measured in the three main areas (Fig.17) does not show sharp differences between the different zones but it demonstrates slight prevalence at the abdominal area after one hour which decreases a bit at the expense of the pelvic area 24 hours later, suggestive of displacement in the direction of the uterus.

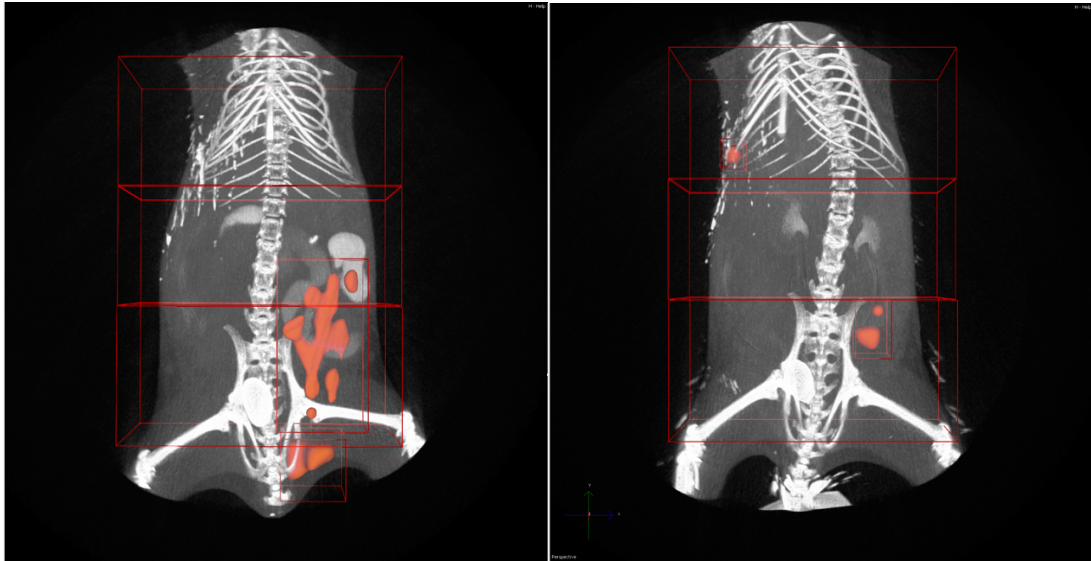


Fig.16. 3D fluorescent imaging performed 1 hour (left image) and 24 hours (right image) after the intraperitoneal injection of the AF750 labeled bacterial ghosts on the treated tumor bearing mouse MCT-0280 imaged in supine position with applied ROIs sets. For optimal 3D visualization is used surface mode provided by the software.

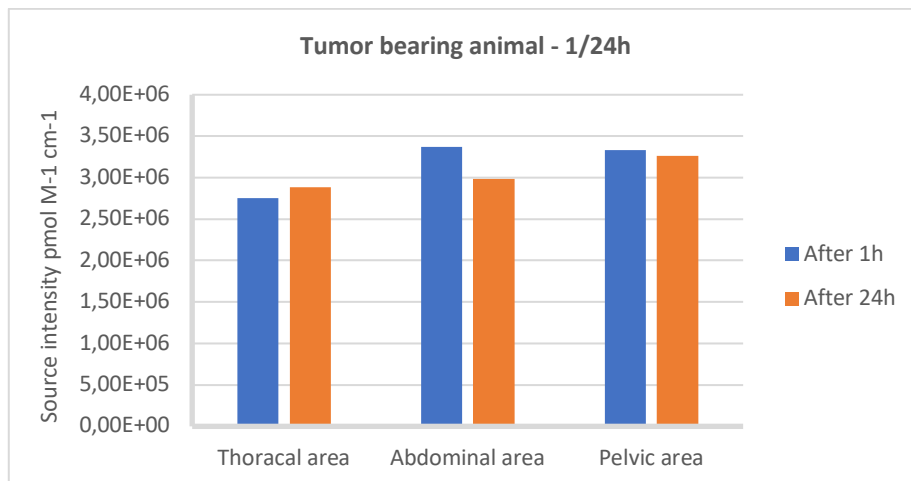


Fig.17. Graphical representation of the total values measured in the thoracal, abdominal and pelvic areas of MCT-0280 1 hour and 24 hours after intraperitoneal injection of the AF750 labeled bacterial ghosts.

Twenty-four hours after the injection, the mice were sacrificed. For validation of the observations made during the FLIT analysis, the organs were carefully removed and imaged. The organ validation revealed presence of pancreas tumors with different sizes in each animal involved in this round, except for the control mice and in addition a colon tumor was found in MCT-0271. The results expose indicatively high signal coming from the tumors, referring to the ability of the BGs to target preferably carcinomas originating from hard-to-reach organs like colon, pancreas, duodenum (Fig.19). A detailed analysis of the organs of the particular animal selected as an example (Fig.18) shows extremely high total radiant efficiency at the pancreatic tumor – 3.11E+09 which is the third highest measured value after the

gastrointestinal tract - $7.15E+09$ and the uterus with its associated fat – $3.49E+09$. Even though, a brief comparison of detected intensity versus total area of the organ disclosed that the most significant concentration is exactly in the cancerous tissues. These observations apply completely to all six tumor bearing mice with single cases with significantly increased signal in the kidneys or in the liver. Lymph nodes from two of the animals were successfully removed and imaged, revealing considerable signal with average measured values of the total radiant efficiency of $5.43E+08$. The graphical representation of the average total radiant efficiency measured in the organs of the tumor bearing animals discloses that the highest signal originates from the gastrointestinal tracts of the mice, followed by significant intensity coming from the uterus, the pancreas, the tumors associated to the pancreas and the liver (Fig.19). It should be borne in mind that, although smaller in size, the cancerous tissues have a very high intensity compared to the whole organ from which they originate.

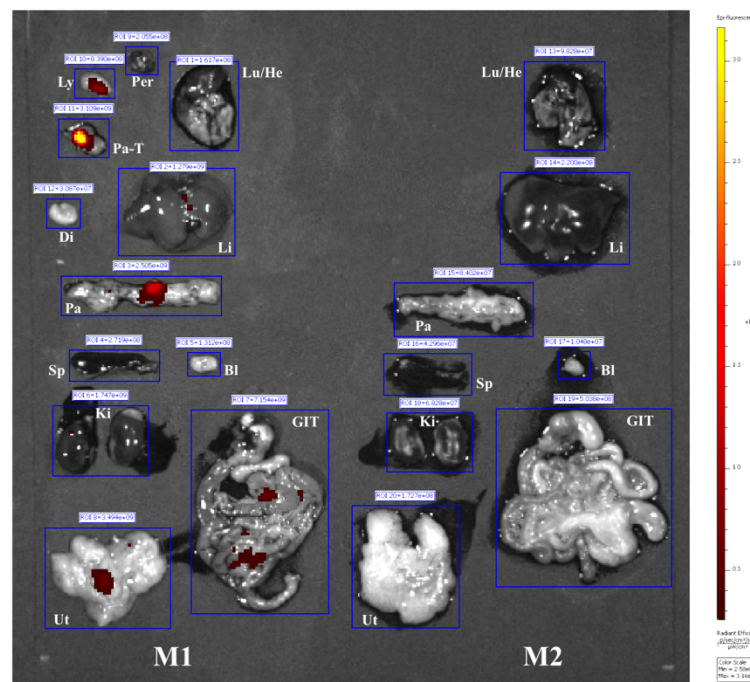


Fig.18. 2D fluorescence organ imaging twenty-four hours after the intraperitoneal injection of AF750 labeled bacterial ghosts. The organs of the non-tumor bearing mouse (M1: MCT-0279) are shown on the left side and the organs of the reference mouse (M2: MCT-0274) are on the right side. The threshold is based on the referent animal. Labels legend: Lu/He = Lung/Heart, Ly = Lymph node, Pa-T = Pancreas tumor, Di = Diaphragm, Li = Liver, Per = Peritoneum, Pa = Pancreas, Sp = Spleen, Bl = Bladder, Ki = Kidneys left/right, Ut = Uterus, GIT = Gastrointestinal tract.

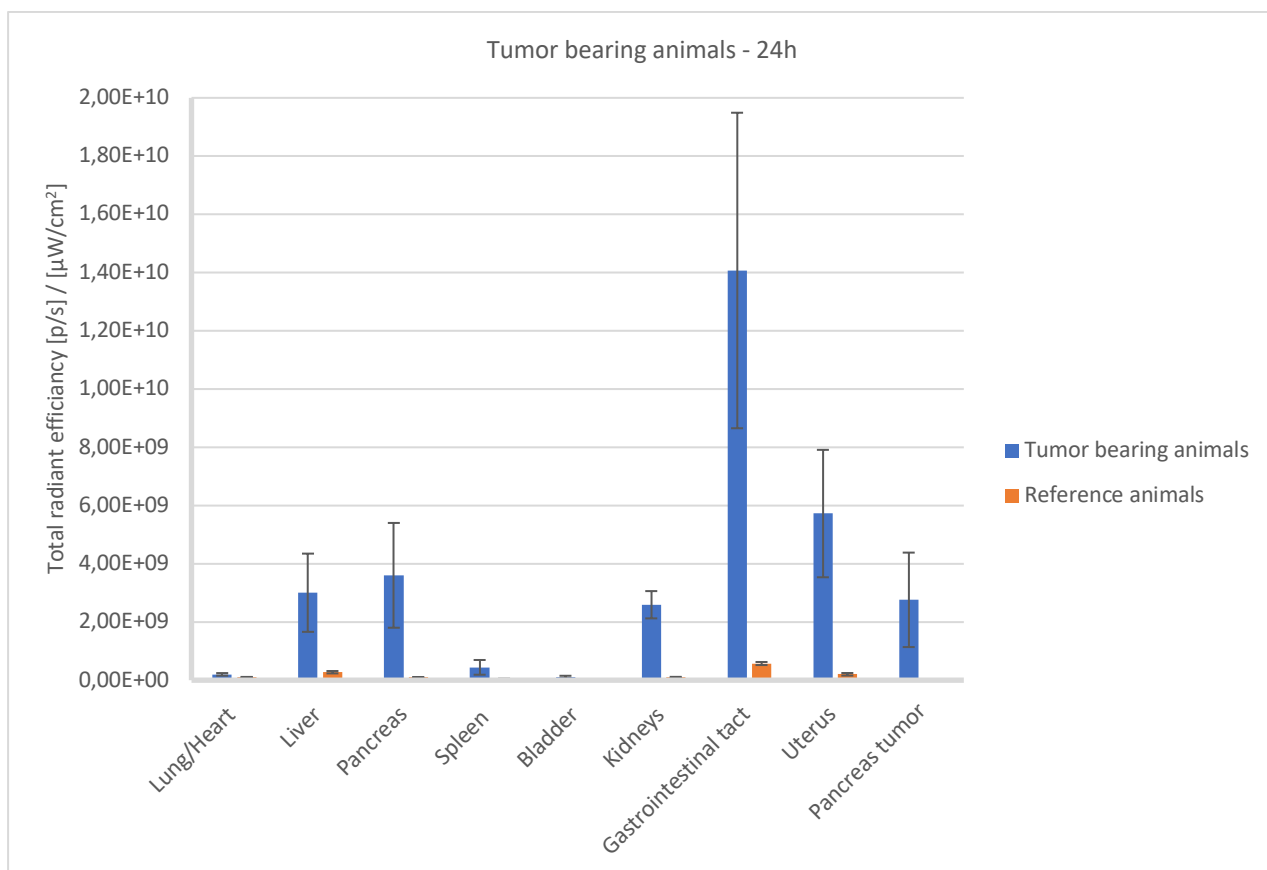


Fig.19. Graphical representation of the average intensity of the organs of mice MCT-0271, MCT-0272, MCT-0273, MCT-0278, MCT-0279, MCT-0280 and the reference mice MCT-0265, MCT-0266, MCT-0274 are shown. The imaging was done twenty-four hours after the administration of BG-AF750.

5.2. Biodistribution of siRNA

In order to investigate the biodistribution of intratracheal delivered NIR-dye labeled siRNA, two different imaging methods were used – 2D epifluorescence and 3D FLIT. Various excitation/emission filters were used for the 2D fluorescence imaging performed in the epifluorescence mode and the most suitable for the used dye (Alexa Fluor 750) was chosen for visualization of the results - excitation filter 745nm and emission filter 800nm. Two non-tumor bearing Balb/c mice were used for the experiment – MCT-0209 and MCT-0215 and they were imaged in prone and supine position at two time points – immediately after the application of the formulation and 24 hours afterwards, which applies for both methods. Two sets of ROIs were created respectively for the two groups of images. The total pmol per ROI were quantified. The dimensions of the zones of interest are absolutely identical for all images of one group and they are also positioned in the most similar manner possible with a mandatory condition to fence the strong signals. Twenty-four hours after the intratracheal pulmonary delivery of AF750-labeled siRNA and the 2D and 3D imaging, the mice were sacrificed under

anaesthesia by cervical dislocation, the organs of interest were carefully removed and imaged for organ validation.

5.2.1. 2D fluorescence imaging of AF750-siRNA

The analysis of the 2D fluorescence data is based on the total radiant efficiency measured at the zones with visualized strong signal, in particular - lungs and kidneys. As a first-round analysis, ROIs were applied only to the areas with obvious signal and no additional assumptions were made, respectively, ROIs were not placed on the presumed positions of the kidneys if there are not any detected fluorescence. ROIs were also not placed around the trachea, despite the obvious fluorescence, because the administration method was taken into account – immediately after the intratracheal delivery a large amount of the siRNA formulation remains in the trachea and this is the reason for the strong signal in this area in supine position at 0h time point and the gradual decrease after 24 hours. The detected signals in the area of the bladder and the rectum (Fig.21. right) were covered in order to detect and image weaker signals coming from other organs. In order to estimate the effect of the strong fluorescence originating from the administration and excretion pathways and to avoid supposed coverage of the signals of interest by them, at some of the images (Fig.22, Fig.23) the excess areas are covered with black type. The result after trying this technique is that the covered mouse MCT-0215 showed higher intensity at the lung ROI – $2,71E+09$ in comparison to the lung ROI of the non-covered MCT-0209 with total radiant efficiency of $3,93E+08$. To the hypothesis about the impact of closely located signals may be added the images of both animals made in prone position (Fig.20, Fig.22) - although the measured value in the lungs after 24h is higher than the one measured at time point 0h, in the images with fluorescent kidneys the signal from the lungs is slightly blunt. Despite the importance of this observation, this experiment does not include the required number of experimental animals and further investigation is required to confirm the impact of the highly fluorescent zones on the intensity of nearby regions. Each image from this 2D round of analysis was subjected to slight adjustments in order to accurately capture the true positive signal. The changed settings include adjustment of the minimum and the maximum of the color scale and alteration of the smoothing and binning.

The results based on the generated 2D data show a clearly outlined distribution pattern (Fig.24) – the intratracheal delivery method ensures immediate access of the AF750-siRNA formulation to the lungs and according to the measured values - 24 hours later the concentration in the lungs is getting even higher as a result of the subsequent distribution of the amount initially found in the trachea. The second well visualized recurring event is the appearance of

significant signal in the kidneys, 24 hours after the administration, indicating for air to blood transfer followed by renal excretion.

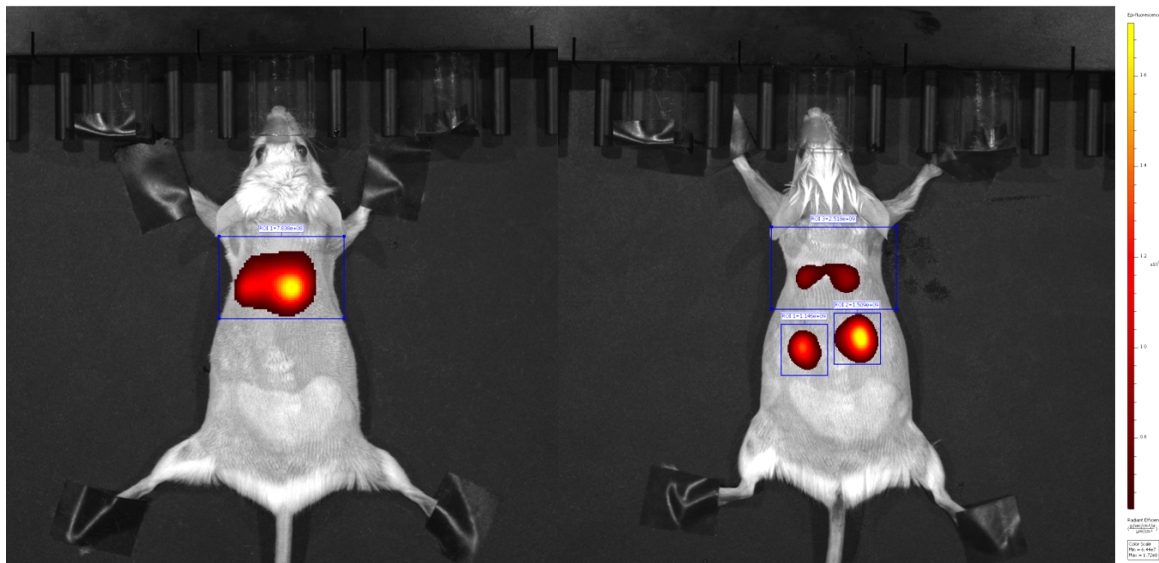


Fig.20. 2D epifluorescence imaging performed 0h (left) and 24h (right) after intratracheal pulmonary delivery of AF750-labeled siRNA. The images present the treated mouse MCT-0209 in prone position. Sets of ROIs were applied on the areas with strong signal – lungs and kidneys and the color scales were adjusted for better visual representation.

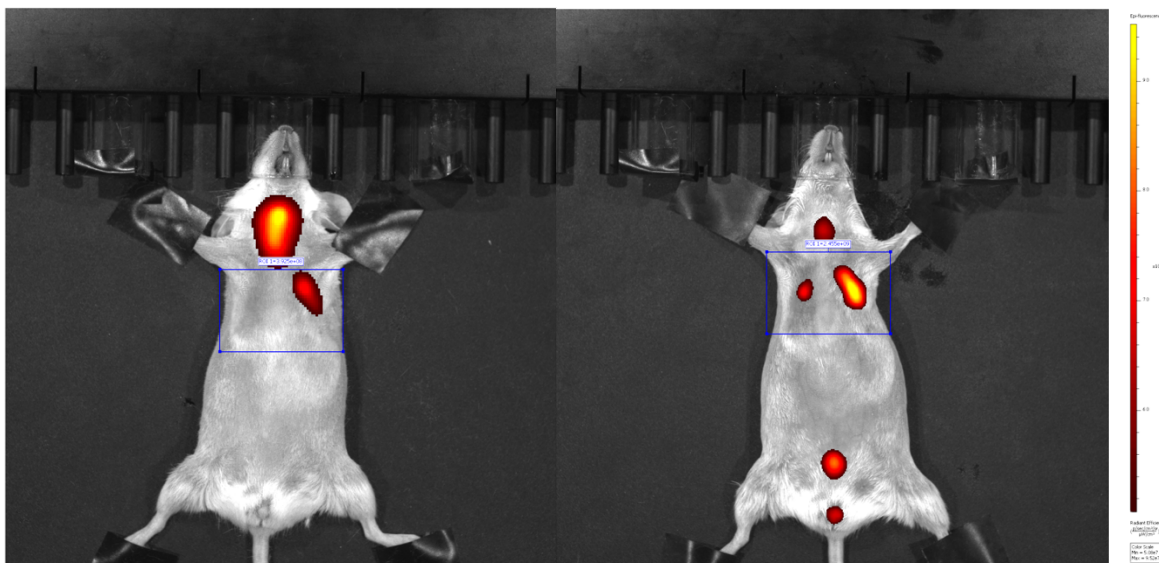


Fig.21. 2D epifluorescence imaging performed 0h (left) and 24h (right) after intratracheal pulmonary delivery of AF750-labeled siRNA. The images present the treated mouse MCT-0209 in supine position. Identical ROIs were applied around the lungs and the color scales were adjusted for better visual representation.

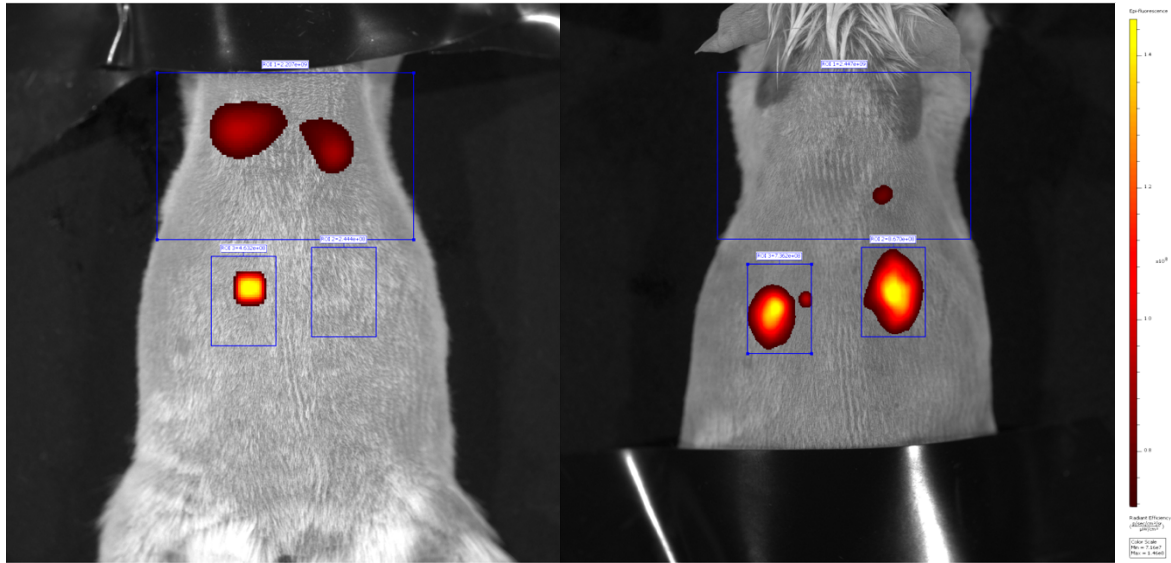


Fig.22. 2D epifluorescence imaging performed 0h (left) and 24h (right) after intratracheal pulmonary delivery of AF750-labeled siRNA. The images present the treated mouse MCT-0215 in prone position. Identical sets of ROIs were applied on the areas with strong signal – lungs and kidneys and the color scales were adjusted for better visual representation.

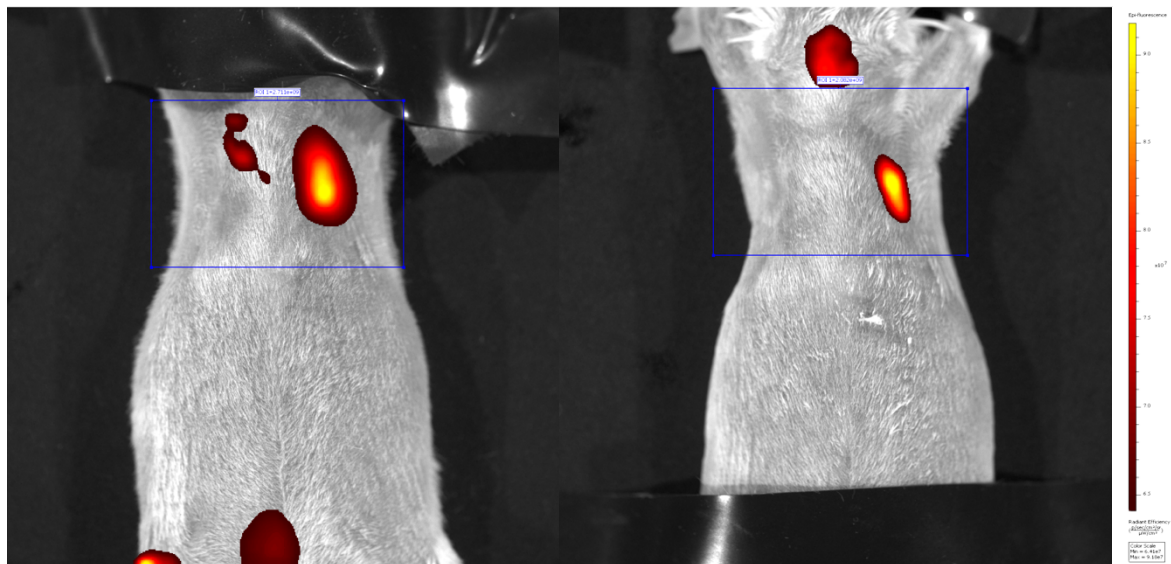


Fig.23. 2D epifluorescence imaging performed 0h (left) and 24h (right) after intratracheal pulmonary delivery of AF750-labeled siRNA. The images present the treated mouse MCT-0215 in supine position. Identical ROIs were applied around the lungs and the color scales were adjusted for better visual representation.

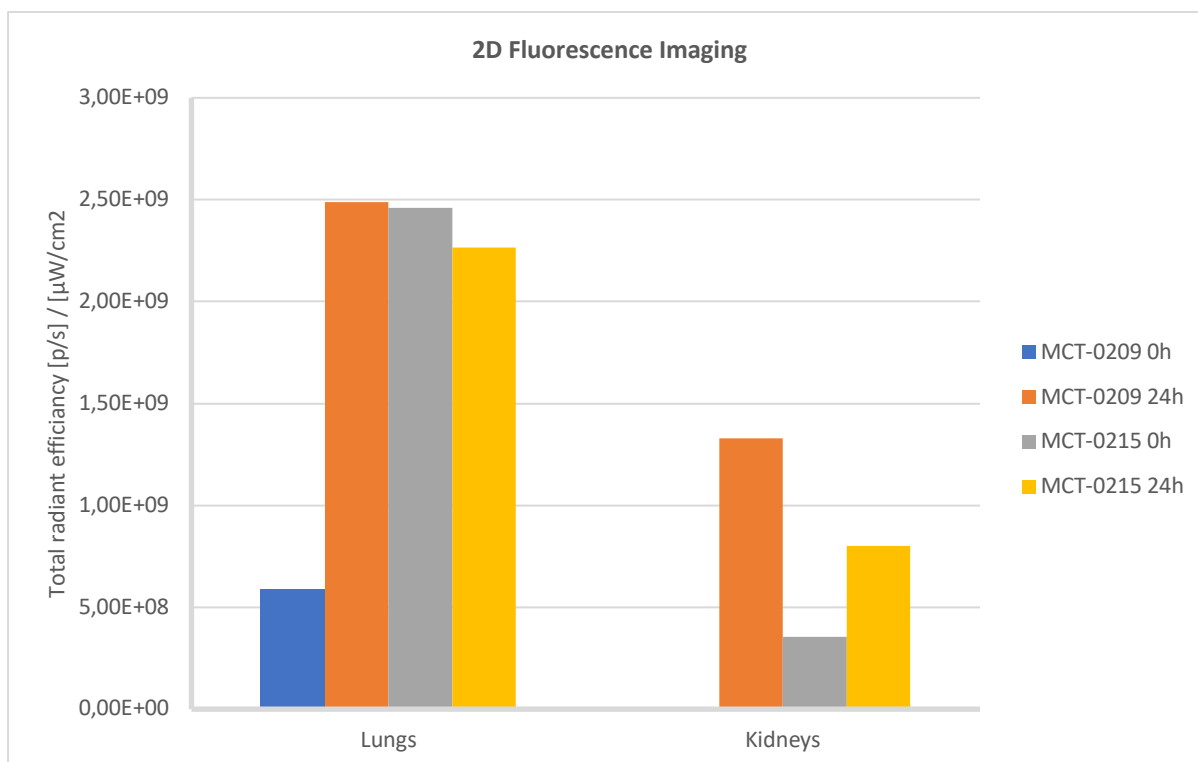


Fig.24. Graphical representation of the total radiant efficiency measured at the regions with detected signal in both mice – MCT-0209 and MCT-0215, immediately after the intratracheal pulmonary delivery of AF750-labeled siRNA and 24 hours after the administration.

For maximum accuracy in present data analysis, should be taken into consideration that the 2D imaging strategy is able to offer only semi-quantification due to some limitations such as increasing tissue absorption for deeper lying signals. This statement can be illustrated by simple comparison between the images at prone and supine position at time point 24h – strong and persuasive signal is recorded in the kidney areas unlike what is seen at supine position with the same animal. For absolute quantification and validation of the already made observations a 3D FLIT procedure was applied.

5.2.2. 3D FLIT of AF750-siRNA

The analysis approach of the 3D FLIT data slightly differs from the one used for the 2D data as we already have starting points and guidelines, identified during the 2D round. The 3D fluorescence imaging tomography of mice MCT-0209 and MCT-0215 was performed immediately after the intratracheal pulmonary delivery of AF750-labeled siRNA and 24 hours after the administration in both prone and supine position. The applied set of ROIs is identical for each of the images and includes a whole-body ROI, software background ROI with the same dimension as the whole body once, lung ROI, left kidney ROI and right kidney ROI (Fig.25). The exact total values measured in the background ROIs and their respective whole-

body ROIs are presented in the section “Materials and methods”. For an accurate interpretation of the results, it should be mentioned that despite their identical shape and size for each image, the exact positions of the ROIs are adjusted according to the positions of the bodies and every image is characterized by slight differences. Should be taken into account that one of these characteristics is the location of the whole-body ROI and more precisely – the upper end of this ROI which is positioned below the trachea in some of the cases, and consequently the amount of AF750-siRNA remained there as a result of the administration method is not always measured. In order to achieve better visualization and to focus on the detected signal, the results are illustrated with images in surface mode and display only the ROIs surrounding the areas with visible signal (Fig.26 and Fig.27). The conclusions made on the basis of displayed fluorescence are a recurrent pattern in both 2D and 3D – at time point 0h there is no visible signal in the kidneys, whereas 24 hours later the signal in this area is strong and clear. However, guided by the observations made during the analysis of the 2D data, ROIs were drawn also around the kidneys even if there is a lack of visual signal, and the total value was measured at every of the listed above regions (Fig.25).

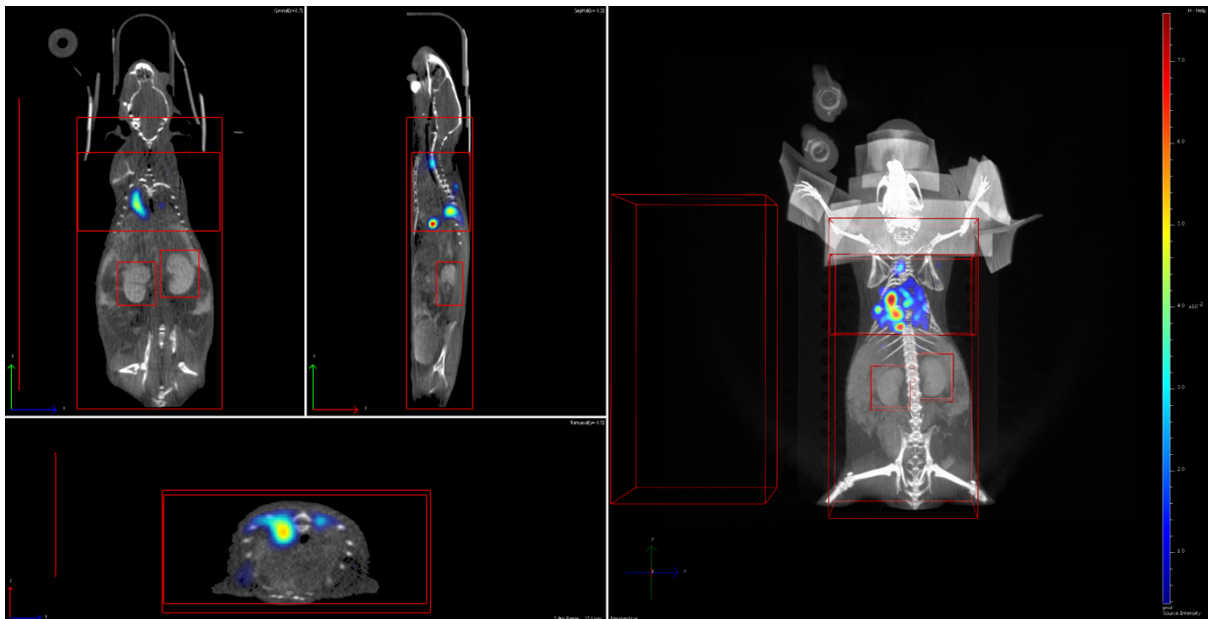


Fig.25. 3D fluorescence imaging performed immediately after intratracheal pulmonary delivery of AF750-labeled siRNA. The images display the treated non-tumor bearing mouse MCT-0209 in prone position with all applied ROIs, in the original view provided by Living Image 4.5.1 software without setting changes.

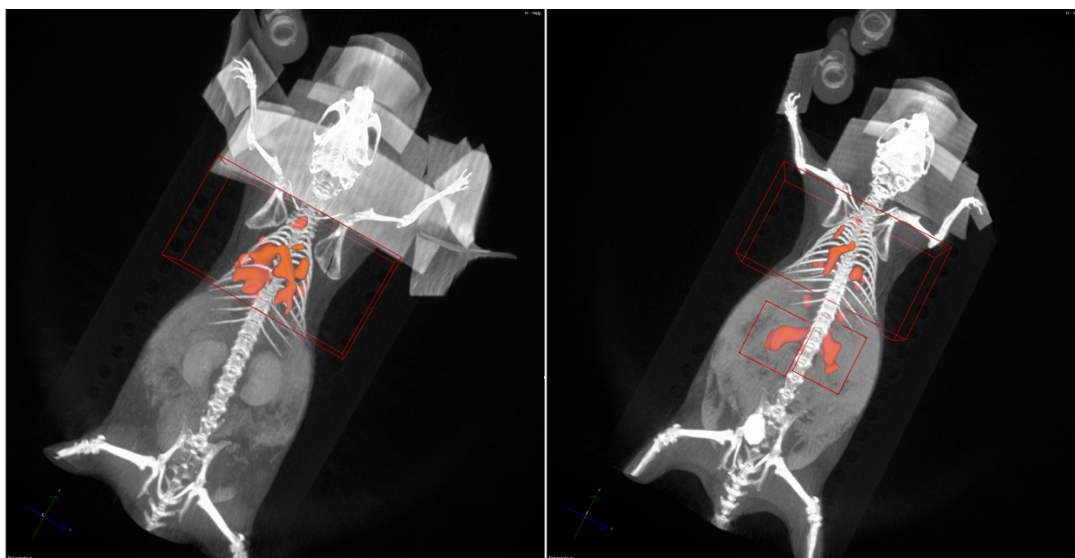


Fig.26. 3D fluorescent imaging performed immediately after administration (left image) and 24 hours (right image) after the intratracheal pulmonary delivery of AF750-labeled siRNA on the treated non-tumor mouse MCT-0209 imaged in prone position with applied surface displaying mode and ROIs sets. The original threshold settings are used, the voxel minimum is set at $1.21e-2$ for 0h image and $1.82e-2$ for 24h image.

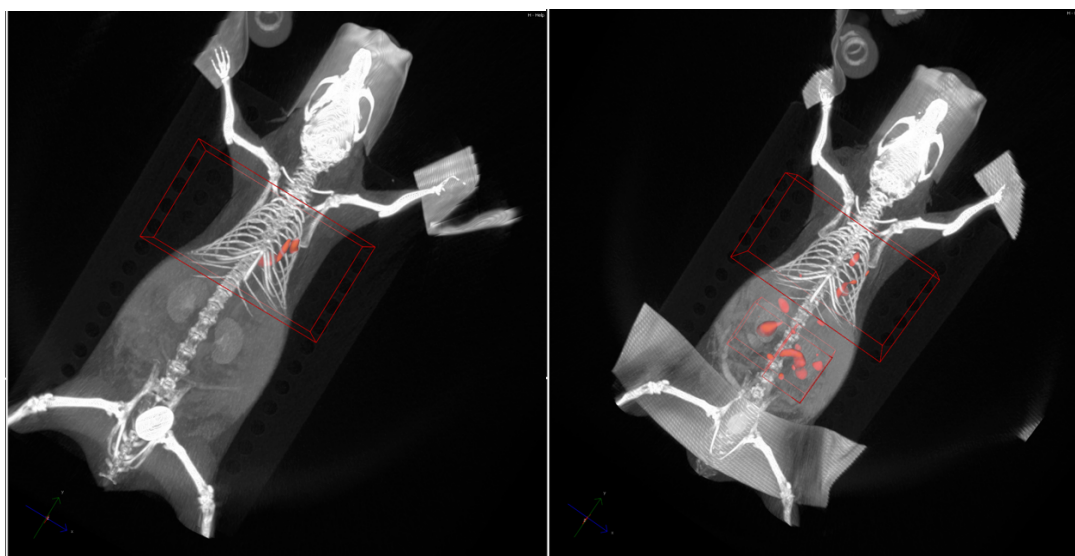


Fig.27. 3D fluorescent imaging performed immediately after administration (left image) and 24 hours (right image) after the intratracheal pulmonary delivery of AF750-labeled siRNA on the treated non-tumor mouse MCT-0215 imaged in supine position with applied surface displaying mode and ROIs sets. The original threshold settings are used, the voxel minimum is set at $3.77e-2$ for 0h image and $1.81e-2$ for 24h image.

When plotted the total values measured in the lungs and the kidneys reveal a trend that slightly differ from the visual assessment of the imaging data - summarized values of the left and right kidney at time point 0h completely coincide with those measured 24 hours later (Fig.28). Confirming the observation linked to the distribution in the lungs, the graphic also shows slight increase of the concentration 24 hours after the intratracheal delivery of the formulation, as a result of the gradual movement through the respiratory tract. Another recurring event ascertained during the FLIT analysis is a modest increase in the measured amount of AF750-siRNA in the bodies of both animals, imaged in both prone and supine

position 24 hours after the administration. The average whole-body total value of $3,11\text{E}+06$ estimated at time point 0h rose up to $3,34\text{E}+06$ at time point 24h. This could be explained by the above-mentioned placing of the corresponding ROI at the lower end of the trachea and not covering the whole one, respectively the signal that was not detected initially migrated down in the lungs upon the second measurement and was caught by the ROIs. The whole-body rates are normalized by subtracting the control ROIs values, aiming to demonstrate the minor impact of the software background, in accordance to the approach applied to the BG project. A comparison between the values before and after subtraction of the control measurements, respectively $3,13\text{E}+06$ and $3,11\text{E}+06$ for the time point 0h, proves that the background noise emanating from the software has no effect on the terminal outputs due to its insignificants.

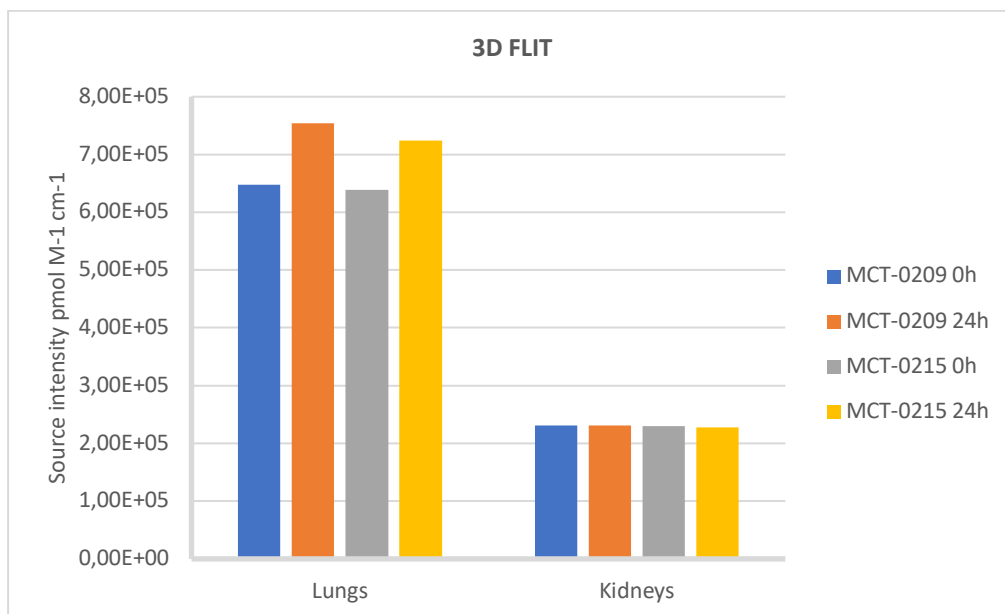


Fig.28. Graphical representation of the total value measured at the regions with detected signal in both mice – MCT-0209 and MCT-0215, immediately after the intratracheal pulmonary delivery of AF750-labeled siRNA and 24 hours after the administration.

5.2.3. Organ Imaging of AF750-siRNA

Twenty-four hours after the intratracheal pulmonary delivery of AF750-labeled siRNA, the mice were sacrificed under anesthesia by cervical dislocation. For validation of the observations made during the 2D and FLIT analysis, the organs were carefully removed and imaged. The imaged organs are lung, liver, gastrointestinal tract, spleen, left kidney and right kidney (Fig.29). The validation results partially coincide with the observations already made – the image of MCT-0209 displays indicative fluorescence in both kidneys and significant prevalence in the lungs. Whereas in MCT-0215 additional signals are detected in the liver and in gastrointestinal tract as well, contrary to the conclusions reached so far.

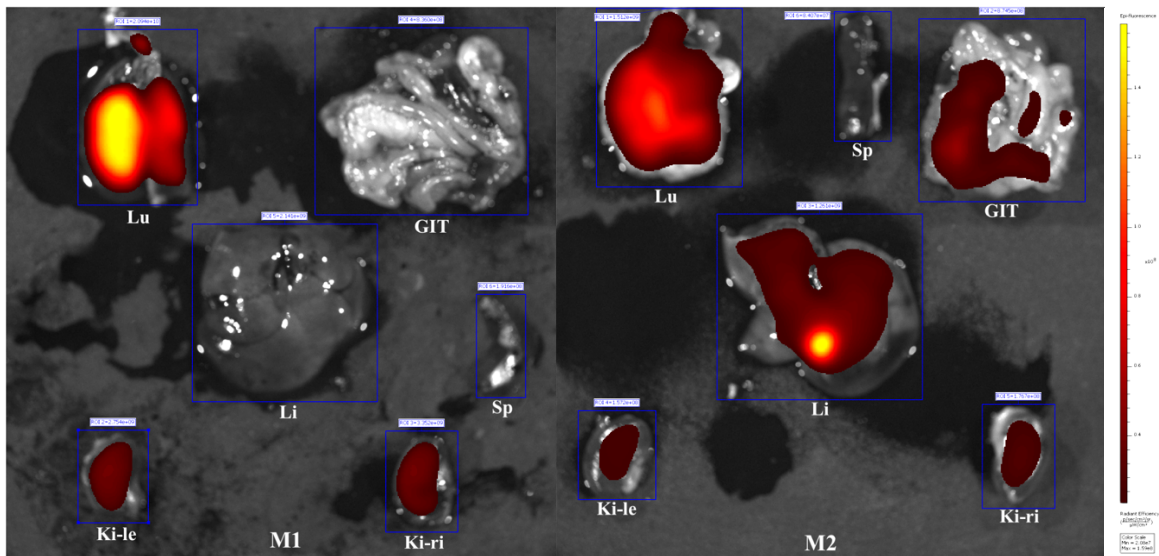


Fig.29. 2D fluorescence organ imaging twenty-four hours after intratracheal pulmonary delivery of AF750-labeled siRNA. The organs of mouse MCT-0209 (M1) are shown on the left side and the organs of mouse MCT-0215 (M2) are on the right side. Color scale adjustments – M1: the minimum is changed from $1.02e8$ to $1.32e7$ and the maximum is changed from $2.00e9$ to $4.56e7$; M2: the min is changed from $8.82e6$ to $2.08e7$ and the max is changed from $1.73e8$ to $1.59e8$. Labels legend: Lu = Lung, Li = Liver, Sp = Spleen, GIT = Gastrointestinal tract, Ki-le/ri = Kidney left/right.

The chart presenting the average of the total radiant efficiency of the both mice's organs demonstrates eloquently the high preference of the administrated formulation to the lungs, followed by high concentration in the kidneys. Furthermore, non-negligible signal is detected in the other organs – liver, gastrointestinal tract and spleen (Fig.30).

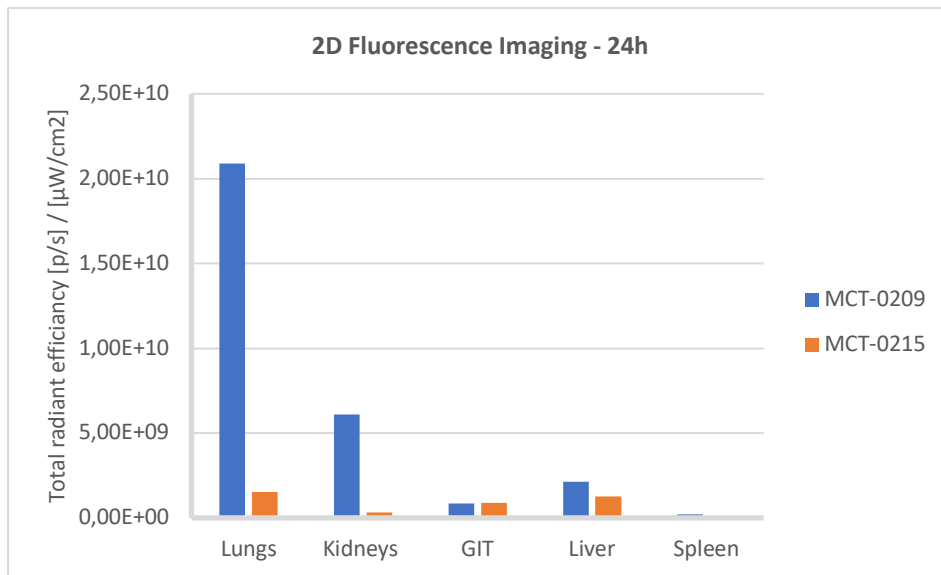


Fig. 30. Graphical representation of the average intensity of the organs of mice MCT-0209 and MCT-0215. The plotted value which presents the kidneys is a summary of the total radiant efficiency measured in both kidneys. The imaging was done twenty-four hours after the administration of AF750-siRNA.

Although the output of the three methods used to track the biodistribution of the AF750 labeled siRNA led to the generalized assumption that the signal comes mainly from the lungs, but further investigation is required because of the small number of experimental animals that participated in this study and the slight mismatch of the 2D and FLIT results with the organ validation of one of the mice.

6. Conclusion

The imaging data generated by two different experiments were analyzed in the present work— tracking the biodistribution of AlexaFluor 750-labeled bacterial ghost and AlexaFluor 750-labeled siRNA. The same software was used to analyze the outcome of both experiments - Living Image 4.5.1 and three different methods were applied for the siRNA tracking – 2D epifluorescence imaging, 3D FLIT and organ imaging, while only 3D FLIT and organ imaging were utilized for tailing the BGs. It is known that the two performed experiments also differ in the chosen method of administration – intraperitoneal injection with bacterial ghosts and intratracheal pulmonary delivery of siRNA. For the bacterial ghost experiment are used non-tumor bearing mice and tumor bearing mice aiming to investigate if BGs have any preference for tumor association, in addition to the biodistribution examination. Whereas, the siRNA investigation involves only two non-tumor bearing animals as it is a pilot experiment and aims to determine the parameters for further study.

The bacterial ghost experiment was divided into three sub-experiments – non-tumor bearing animals imaged 2 hours after the administration, non-tumor bearing animals imaged 1 hour and 24 hours after the administration and tumor bearing animals. Two hours after the intraperitoneal injection, ghosts are almost evenly distributed into the three pre-selected ROIs/body areas – thoracic, abdominal and pelvic. The generated 3D images display signal in the gastrointestinal tract, in the liver and in the uterus with discrepancy between the two tested animals. The organ validation done 5 hours after the administration confirms these measurements with its two peaks in the liver and uterus. The second round also include two tumor free mice but imaged at two different time points, giving a clearer idea of the movement of the formulation. Results reveal that one hour is enough for wide spreading of the ghost within the whole body with dominance of the signal in the abdominal area and more precisely, the preference seems to be for the pancreas and intestines. Twenty-four hours later the signal detected in the pancreas remains significant, whereas the BGs from the gastrointestinal tract have migrated to the uterus and the fat around the uterus, shifting the peak to the pelvic area. The organ imaging validates the results, exhibiting highest signal in the pancreas and the uterus, followed by the gastrointestinal tract and the liver. The third sub-experiment includes 6 tumor bearing BG-injected animals, five of which are imaged 24 hours after the delivery of the formulation, and one is imaged 1 hour and 24 hours after the administration. The presented results are consistent with the observations made so far – 24 hours after the intraperitoneal injection the concentration of ghosts is highest in the pelvic area. Due to the inclusion of more

experimental animals in this round, the individual analysis of each one of them and the determination of the fluorescent organs led to slightly heterogeneous observations – the 3D images displayed visual signal in different organs such as kidneys, liver and intestines in addition to the already mentioned pancreas and uterus but still most often the identified parts are exactly the gastrointestinal tract, the uterus and the pancreas. The organ validation evidenced for significant signal in the tumor tissues samples, colon cancer and pancreatic cancer in the particular case, and consequently the highest total radiant efficiency were measured in the gastrointestinal tract. A summary of the three rounds led to the conclusion that BGs show preferences to tumor tissues, pancreas and uterus, but their distribution affects almost all major organs more or less.

The siRNA experiment is a pilot experiment aiming to outline the biodistribution pattern of the intratracheally delivered AF750-labeled siRNA and to develop a model for analyzing further data. On both experimental mice were performed 2D epifluorescence imaging and 3D FLIT immediately after the administration of the formulation and 24 hours after it. The results eloquently show considerable concentration of siRNA at the lung which remains unchanged for the 24 hours of the observation, followed by significant signal in the kidneys which subjects for the most likely route of excretion of the substance. The organ validation confirms the reached conclusions.

Last but not least, a subject of interest of the experiments listed above was also the assessment of the 2D and 3D FLIT options provided by Living Image in the context of sufficient data analysis of *in vivo* biodistribution tracking. The measurements made in each of the tested methods are convincing and are considered to accurately detect total radiant efficiency with minimal and negligible software background noise. On the other hand, visual representation of the signal in some cases omits zones with a fluorophore concentration that is relevant to the experiment. The discrepancies appear rather in the FLIT analysis. However, the information generated in the form of images is sufficient to direct the study to the organs with the highest content of fluorescent agent and this was proved by organ validation. Despite the need for improvements, the FLIT method allows deeper penetration and thus minimizes the 2D surface imaging limitations. It also enables a more precise identification of the organs of interest. Advantages of the software are the tools that allow the presentation of the visual information in a clear and suitable for publication form.

7. ADDENDUM

7.1. Introduction

Earlier in this work, the principle, the application and the importance of bioluminescence and fluorescence imaging were discussed. The combination of the significant improvement of the *in vivo* imaging methods and the progress made in gene manipulation resulted in creation of transgenic reporter animal strains with different investigation purposes like studies of particular tissues, assessment of delivery systems and direct monitoring of tumor in its natural environment.

Bioluminescence imaging is a typical example of a completely biological process existing in nature, turned into an excellent tool for scientific needs. The combination of key elements including the enzyme luciferase, a substrate, oxygen and some co-factors lead to light-producing chemical reaction in living organisms which in turn has become an essential tool for noninvasive monitoring of biological processes *in vivo* (Badr & Tannous, 2011). After the successful cloning of the firefly luciferase in the second half of the 20th century, it immediately became preferred instrument for use in gene regulation studies due to the lack of post-translational modifications (Sadikot & Blackwell, 2005). The luciferase genes that have been cloned so far can have different origin - from bacteria, insects, and marine organisms but the luciferase from firefly (*Photinus pyralis*) is the most widely used a report gene in mammalian cells (Bauer P., 2011).

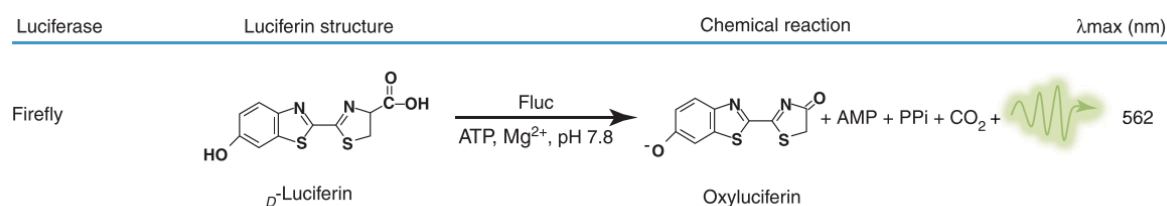


Fig.31. Chemical reaction of firefly luciferin to oxyluciferin and light emission at 562nm wavelength (Badr & Tannous, 2011)

Luciferase reporter gene assays have multiple application in biomedical science and especially in cancer biology. Initially they were used for mapping and characterizing transcriptional control elements including monitoring the effect of siRNA-mediate inhibition of specific factors. Another important application is in the study of particular components

involved in signaling pathways upstream of transcription such as protein kinases or cell-surface proteins. Combined with cell-based highthroughput screening the luciferase reporter gene is suitable for identification of activators or inhibitors of drug targets which makes it of great benefit for the drug discovery programs. Last but not least, it is the exciting use in visualization of gene expression *in vivo* – the already discussed bioluminescent imaging. For these non-invasive *in vivo* assays two main options have been described – assay performed on animals injected with cells or virus containing luciferase reported gene or by utilizing a luciferase reporter gene transgenic animal (Bauer P., 2011).

Over the decades, the transgenic methodology has become an indispensable tool for building genetic disease models and investigating the genetic control of physiological systems. Transgenic animals can be produced via several different methods, including virus-based transfer of DNA, liposome-mediated DNA transfer, embryonic stem cells injection, electroporation of DNA, exogenous DNA transfer and the most widely used - microinjection of genes into pronuclei (Wheeler, Walters, & Clark, 2003). The procedure for the production of transgenic mice is relatively costly, technically demanding and it takes approximately a year. In a very brief version, it can be summarized that the main steps include making the fusion DNA construct containing the coding sequence, harvesting fertilized ova from superovulated female mice, injecting the DNA into the pronucleus of the zygotes and reimplanting the injected zygotes. The process is considered to be successfully completed after genotyping and obtaining satisfactory results (Ittner & Götz, 2007). Characteristic of this method is that the microinjected DNA tend to integrate randomly into the genome and as a consequence the levels of expression of the same transgene can vary and there is potential for undesired insertional mutagenesis. However, its advantages are undeniable – lack of limitations with regard to the type or the size of the used constructs, the transgene is transmitted to the next generations and high frequency of generating transgenic animals (Dunn, Kooyman, & Pinkert, 2005).

7.2. Background

The experiment described below was performed thanks to the kind guidance of Mag. Simon Decker.

7.2.1. Aim of the experiment

Three novel transgenic reporter mouse strains have been generated Tg(SftpC Luc)line6, Tg(Thy1.Luc)line7, Tg(Luc705)line1050 for investigation of respectively siRNA mediated knockdown and siRNA delivery in the lung tissues, brain specific drug delivery and evaluation of Splice Switching Oligonucleotides (SSO) formulations. F₀ generation has been generated with pronuclear injection method applied into a zygote of C57BL/6 mice (B6) in the external institute “Institut für Labortierkunde” by Univ. Prof. Dr. Thomas Rüllicke. For further scientific purposes of the Laboratory of Macromolecular Cancer Therapeutics, in the animal facility of the Clinical Pharmacy department F₁ generation has been bred by mating with B6N-Tyrc/BrdCrCl (B6-Alb). The genotype of the animals with one transgenic parent and one wild type parent could be hemizygous transgenic or not transgenic. Homozygous transgenic F₂ generation is a result of mating two hemizygous mice. To confirm the successful inheritance of the gene in the offspring, genotyping of all individuals is required. The protocols for gene extraction and genotypic characterisation of these three novel transgenic reporter mouse strains has been pre-optimized by Sophie Pinczolits (Pinczolits, 2017). The aim of the experiment described below is to determine the presence or absence of the genes of interest in the newly bred animals and to perform a cross-check for validation of the result of the phenotypic assessment.

7.2.2. Gene information

Tg(SftpC Luc)line6 mice were generated for scientific purposes including investigation of siRNA mediated knockdown and delivery studies of siRNA.

The RNAi gene-silencing mechanism is known since the end of 1990s and its natural origin is associated with the normal defense of the organism against viruses and the mobilization of transposons. The process could be briefly explained as a cascade of biochemical events triggered by short double stranded RNAs, involving the specific cytoplasmic ribonuclease III (RNase III)-like protein Dicer and the multiprotein

complex RNA-induced silencing complex (RISC), resulting in posttranscriptional gene silencing by degradation of mRNAs (Leung & Whittaker, 2005).

The used method is by pronuclear injection of plasmid pSPC-Luc-PGL3b with integrated lung specific promotor SP-C and firefly luciferase gene, performed by Biomodels Austria/ Institute for Laboratory Animals Sciences of the University of Veterinary Medicine in Vienna (Fig.32.).

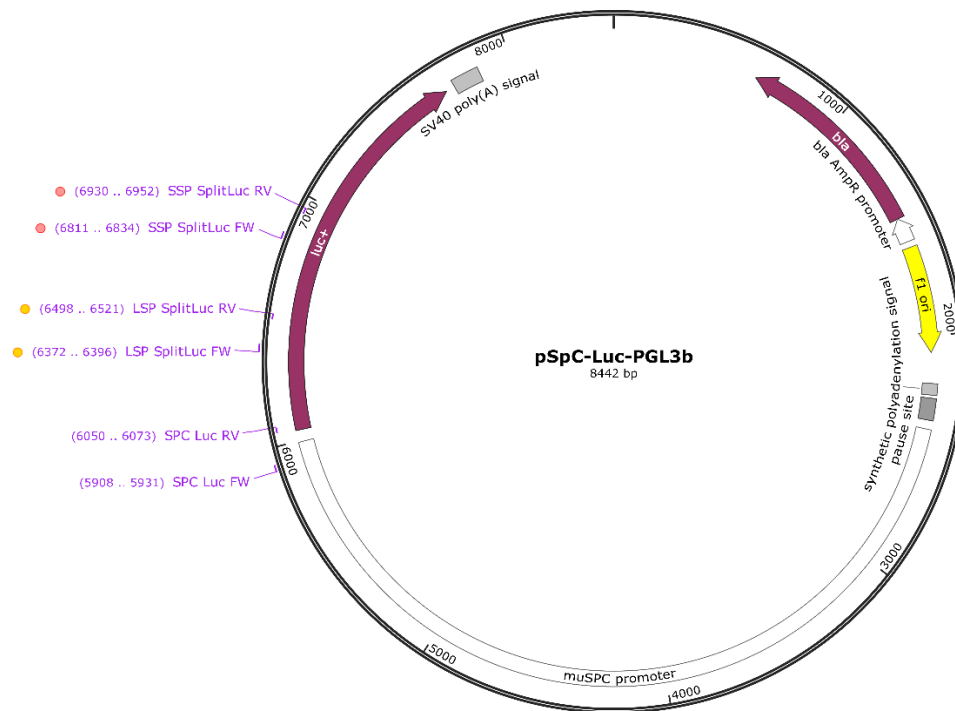


Fig.32. Plasmid map of pSPC-Luc-PGL3b created by SnapGene®

Generation of Tg(Thy1.Luc)line7 has been performed by the same institute as the already mentioned Tg(SftpC Luc)line6 and the same pronuclear injection procedure has been applied. The plasmid construct pThy1.2-Luc-pUC18 used in this particular case contains brain specific promoter Thy1.2 and firefly luciferase gene cloned into the XhoI site of the Thy1.2 expression cassette (Fig.33.). The developed transgenic animals find their application in studies for brain specific *in vivo* drug delivery systems.

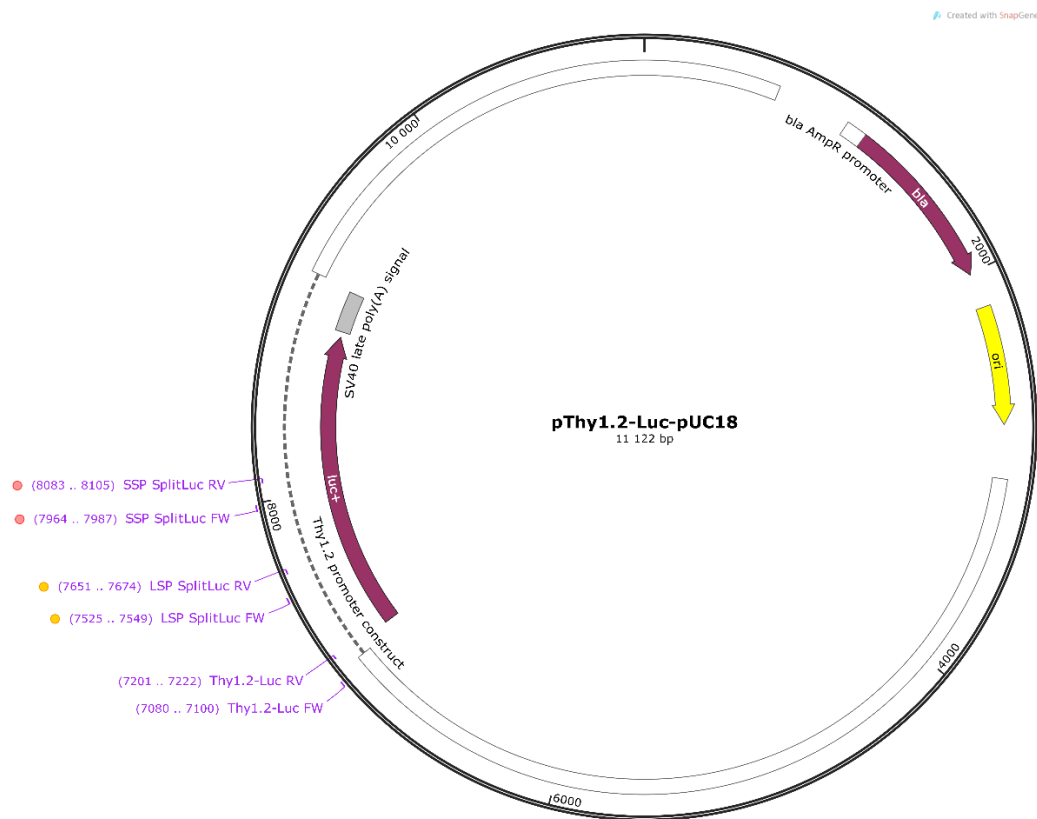


Fig.33. Plasmid map of pThy1.2-Luc-pUC18 created by SnapGene®

The third line of interest in this study has been produced by the same group and under the same conditions as the those already considered. The plasmid construct (Fig.34.) comprises two important specifications – first one on the backbone pBROAD2-mcs which includes Rosa26 promoter and additional regulatory element - β Glo pAn and the second one in on the firefly luciferase gene which contains an aberrant splice site mutation (Resina et al., 2007). The generation of SplitLuc gene bearing animals plays key role in splice correction studies and evaluation of SSO formulations.

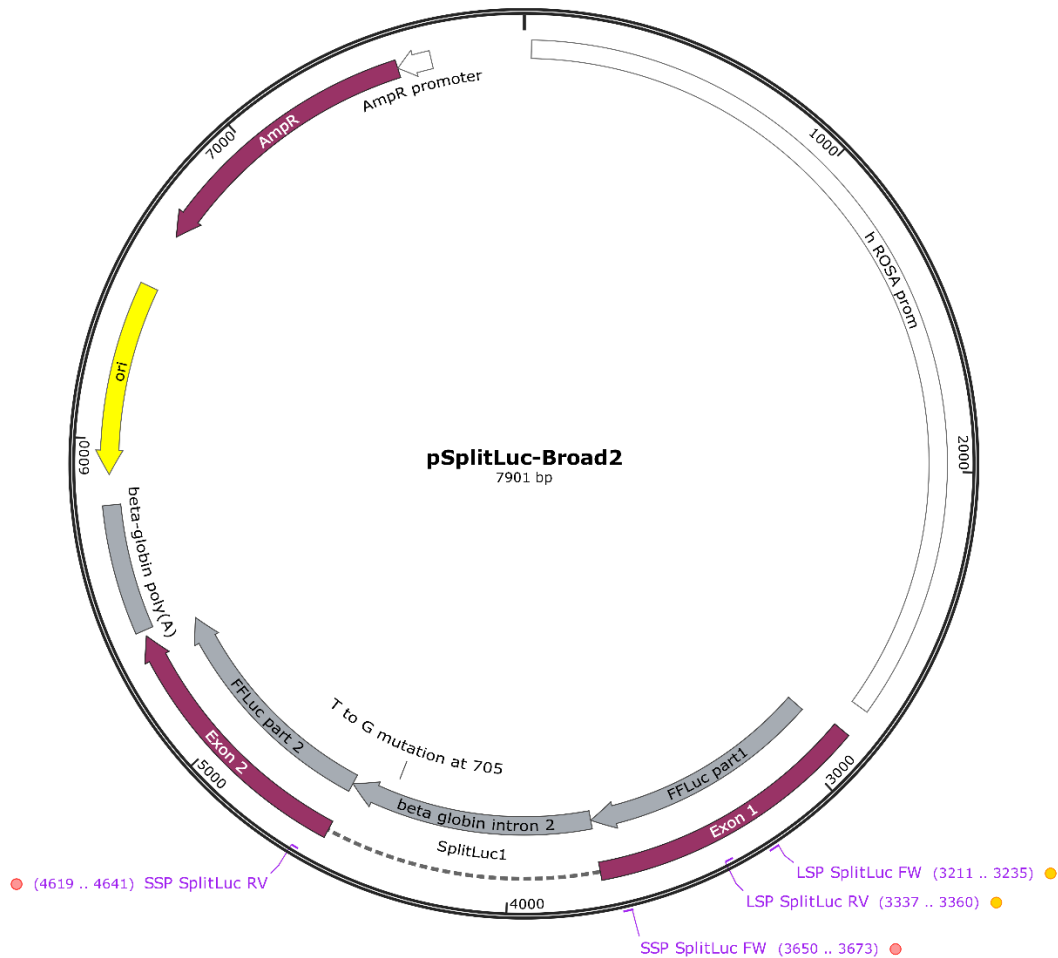


Fig. 34. Plasmid map of pSplitLuc-Broad2 created by SnapGene®

7.2.3. Genotyping

Main steps in the genotyping process include extraction of genomic DNA, performing a polymerase chain reaction (PCR) and outputting results via gel electrophoresis. The biological material used in the current experiment is detached in advance via ear biopsy method with a punching device. The method has been chosen due to its relatively reduced pain and bleeding and performed by the group with access to the animal facility of the MMCT. For the extraction is used commercially available kit. The genotyping itself is performed by standard PCR method. The protocol which was followed has been optimized in advanced by Sophie Pinczolits (Pinczolits, 2017). A real-time PCR is not applied in the present experiment, as the aim is limited to crosschecking for the presence of the genes of interest and quantitative analysis is not required.

Since its development in the 80s of the last century, polymerase chain reaction has become an integral part of the research activities of every laboratory. Its uniqueness is due to the ability to produce million copies of a specific DNA or RNA sequence in an uncomplicated three-step cycling process (National Laboratory of Enteric Pathogens, Bureau of Microbiology, 1991). One cycle usually takes from 3 to 5 minutes and it is repeated from up to 40 times. The steps are denaturation of double-stranded DNA to a single-stranded DNA by raising the temperature to 95°C, annealing of small oligonucleotides of a length of 15-20 nucleotides – primers at 50-65°C, and amplification or extension when the DNA gets doubled by a heat resistant DNA polymerase (Schochetman, Ou, & Jones, 1988). After the amplification of the sequence of interest the PCR procedure is considered as completed and final phase of the genotyping experiment is identification of the product by gel electrophoresis. Agarose gel electrophoresis is a standard procedure for separating DNA fragments of varying sizes ranging from 100 bp to 25 kb. The DNA molecules are separated by size and the distance traveled through the gel in the direction to the positively charged anode is inversely proportional to the log of the molecular weight. After separation, the DNA molecules of interest can be visualized after staining with an appropriate dye (Lee, Costumbrado, Hsu, & Kim, 2012).

7.3. Material and Methods

7.3.1. Gene extraction

Genomic DNA was extracted out of ear punches of the mice of interest. The punches have been taken in advance and preserved frozen into a 1.5ml microcentrifuge tubes. Same procedure was applied for all three lines. Gene extraction was performed with ThermoFisher Scientific GeneJET Genomic DNA Purification Kit #K0721, #K0722, during the procedure Mammalian Tissue and Rodent Tail Genomic DNA Purification Protocol provided by ThermoFisher Scientific was followed. The ear punches were resuspended in 180 μ l Digestion Solution and 20 μ l of Proteinase K Solution were added. Proper closing of the tubes was ensured by wrapping with Parafilm M[®]. The samples were incubated for 16 hours at 56°C and 1500rpm on Eppendorf ThermoMixer[®]. Next step includes adding of 20 μ l RNase A Solution, vortexing and another incubation for 10 minutes at room temperature, followed by adding 200 μ l Lysis Solution and obtaining homogeneous mixture by vortexing. The resulting solution was mixed with 400 μ l 50% ethanol. The obtained lysate was transferred to GeneJET Genomic DNA Purification Column inserted in a collection tube and the column was centrifuged for 1 minute at 6000 x g and the collection tube with the flow-through solution was discarded. Afterwards, the Purification Column was placed into a new collection tube with a capacity of 2ml and 500 μ l Wash Buffer I containing ethanol were added, followed by 1minute centrifugation at 8000 x g. The flow-through was discarded, the column was placed back into the same collection tube, 500 μ l Wash Buffer II containing ethanol were added and another 3 minutes of centrifugation were run at maximum speed of 15000x g. The collection tube with the flow-through solution were once more discarded and the Purification Column was transferred to a new sterile 1,5ml microcentrifuge tube. To the centre of the GeneJet column membrane were carefully added 50 μ l elution buffer, followed by 2 minutes of incubation and 1 minute centrifugation at 8000g. For maximum DNA yield in another tube the elution step was repeated with additional 50 μ l elution buffer and the samples were stored in refrigerator at -20°C for sequent concentration measurement. The samples extracted after the first elution were directly measured.

Genomic DNA concentration of the first elution samples was measured by NanoVue Plus[™] photometer. For proper measurements the plate was cleaned with soft lint-free tissues and deionized water. As reference a 2 μ l drop of the elution buffer from the DNA purification kit was used. After careful resuspension with the pipet, 2 μ l of each sample were applied on the

device and the measurement were performed. DNA concentration was calculated by the absorption at 260 nm, additionally a 260/280 nm ratio of > 1.7 was considered to be pure DNA and a ratio of > 1.7 at 260/230 was evaluated to show minimal presence of sugars, peptides etc.

7.3.2. Polymerase Chain Reaction

The desired concentration of genomic DNA is 5ng/μl and the total amount of Master Mix required for one reaction is 20μl, respectively the data obtained via NanoVue Plus™ photometer was converted and the calculations needed for proper dilution preparations were done. For the procedure is used DreamTaq Green 2X Master Mix by Thermo Fisher Scientific (Ref: K1081). Each sample were tested at least three times to ensure reliable result and some of the samples were tested additionally with GoTaq G2 Hot Start Green Master Mix by Promega for a side experiment aiming to compare both Master Mixes. As a result, it was concluded that DreamTaq Green Master Mix 2X is more suitable for the purposes of the current work.

Master Mix reaction components per a reaction are 0,6μl nuclease free water, 10μl DreamTaq Green 2X, 1μl 5μM primer (not provided in the kit), 0,4μl 25mM additional MgCl (not provided in the kit) which is added to the 2mM included in the kit – a protocol optimization by Sophie Pinczoliths. To the total volume of the mix is added 8μl of the 5ng/μl DNA sample. Apart from the samples of interest, two non-template controls were prepared by adding 8μl nuclease free water and one template control prepared by adding plasmid DNA (10⁴ molecules/μl) was used as positive control. 6X loading dye was used to fill any empty slots in the agarose gel to ensure uniform distribution of the electrical gradient throughout the whole gel. For performing the procedure were used also micropipettes and filter tips, 0,2ml PCR tubes and ice bucket for keeping the samples and the reagents on ice.

Primers used during the study (Pinczoliths, 2017):

Primer Tg(Luc705)line1050 FW 5' TAATGAACGTGAATTGCTCAACAG 3'	Microsynth- The Swiss DNA company	Oligo ID # n/a
Primer Tg(Luc705)line1050 RV 5' TGGTAATCCGTTTTAGAATCCATG 3'	Microsynth- The Swiss DNA company	Oligo ID # n/a
Primer Tg(Thy1.Luc)line7 FW 5' CTGGCTGACCTGTAGCTTTCC 3'	Microsynth- The Swiss DNA company	Oligo ID # 2620706

Primer Tg(Thy1.Luc)line7 RV 5' CTTTATGTTTTTGGCGTCTTCC 3'	Microsynth- The Swiss DNA company	Oligo ID # 2620707
Primer Tg(SftpC Luc)line6 FW 5' CCTGTCCTCTCTGTCTCTGATGAT 3'	Microsynth- The Swiss DNA company	Oligo ID # 2620702
Primer Tg(SftpC Luc)line6 RV 5' CTTTCTTTATGTTTTTGGCGTCTT 3'	Microsynth- The Swiss DNA company	Oligo ID # 2620703

For the execution of the chain reaction itself, BIO-RAD C1000™ Thermal Cycler was used. The protocol includes the following steps – denaturation for 180 sec at 95°C, 34 cycles of Amplification at 95°C for 20 sec each, followed by 60°C for 20 sec and 72°C for 20 sec, final extension at 95°C for 30 sec, followed by 58°C for 120 sec and 72°C for 300 sec and holding at 4°C.

7.3.3. Agarose Gel Electrophoresis

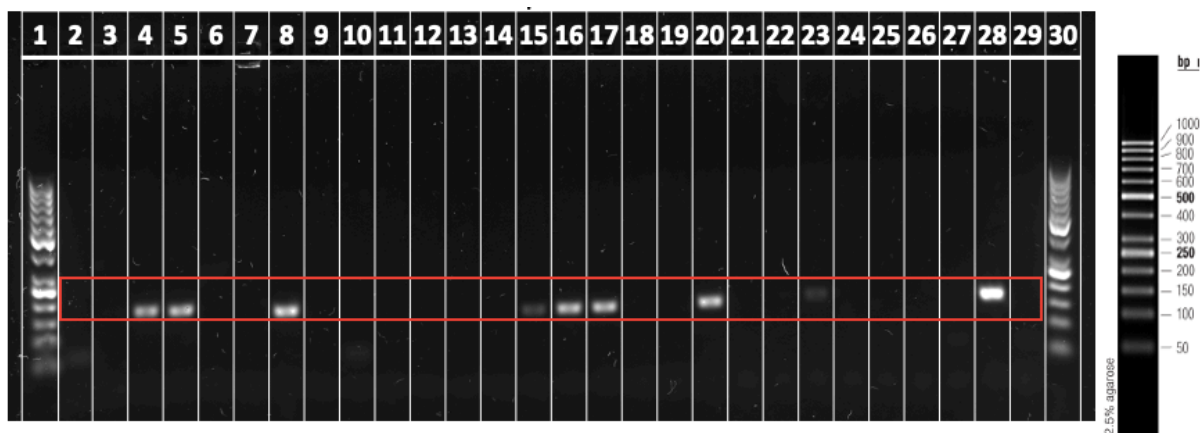
For separating the DNA fragments agarose gel was prepared and an electrophoresis was run. For the purposes of the current experiment 1.5% agarose gel was prepared in an Erlenmeyer flask by mixing 1.8g Agarose SERVA for DNA electrophoresis, 120 ml 1xSB Buffer and 12 µl SYBR Safe DNA gel stain 10,000x concentrate in DMSO. For preparation of 1l 20xSB Buffer concentrate, 8 g NaOH, 48 g Boric acid were dissolved in ddH₂O and filled up to 1l, then 6M HCl was added for adjusting to pH=8. The buffer has been autoclaved. For further use the 20xSB buffer was diluted with MillQ water to 1xSB. The agarose-buffer mixture was heated up gradually in a microwave until it started boiling slightly and the solution was completely clear. Then it was poured carefully in the levelled and locked pouring bed of the gel station with the comb already placed in the corresponding slot. The polymerization of the gel took approximately 20-30 minutes at room temperature. The device used for the electrophoresis is electrophoresis chamber Sub- Cell® GT Horizontal Electrophoresis System by BIO-RAD filled with 1xSB buffer and BIO-RAD PowerPac 200 Electrophoresis Power Supply. Two of the slots of the gel were filled with 4µl GeneRuler 50 bp DNA Ladder by Thermo Scientific and the rest – with 10µl of the DNA samples. After loading all samples, the device was set up at 100V for 45 minutes. For visualization of the stained bands was used ChemiDoc™ Imaging System by BIO-RAD. Different exposure times (3,5s,4s,6s and auto exposure) were set up for achieving best visualization.

7.4. Results and Discussion

All three experiments were repeated three times for ensuring reproducibility and excluding possible false positive or false negative results caused by pipetting mistakes. In addition, the loading positions were changed for every round, once again aiming to avoid mistakes. The intensity of the bands varies, and it is not identical for all samples, however if there is a detected signal in all three rounds of the experiment, the animal is declared as transgenic positive. For more precise estimation different duration of the exposure was tried (3,5sec, 4sec, 6sec) while displaying the results by the imaging system and at some cases this made it possible to notice the weakest signals (Fig.36).

7.4.1. Genotyping of Tg(SftpC Luc)line6

The genotyping procedure described above was applied on 23 potentially transgenic Tg(SftpC Luc)line6 mice. The length of the amplicon of interest is 150bp, respectively as positive are considered the samples which displayed visible band around 150bp (Fig.35). After the analysis of the results as transgenic positive were declared seven mice: MCT-0236, MCT-0239, MCT-0307, MCT-0308, MCT-0311, MCT-0332 and MCT-0333. The negative samples and those that have shown questionable results were tested once more with doubled genomic DNA concentration and all of them were considered as negative. This was the case with MCT-0331 which showed distinctly positive signal after the first round (Fig.35), no-signal at all after the second run and very slight and questionable band after the third round. To clarify the case, the sample was tested again in the control run with doubled concentration and the result showed that the particular mouse was not a transgenic one. Possible reason for the controversial outcome could be a pipetting mistake or an imperfection of the gel. Same positive and negative controls were used for every run and they never gave false positive or false negative result.



1	50bp Ladder	11	27 / MCT-0327	21	37 / MCT-0237
2	NTC - water Split	12	28 / MCT-0328	22	38 / MCT-0238
3	6 / MCT-0306	13	29 / MCT-0329	23	39 / MCT-0239
4	7 / MCT-0307	14	30 / MCT-0330	24	40 / MCT-0240
5	8 / MCT-0308	15	31 / MCT-0331	25	41 / MCT-0241
6	9 / MCT-0309	16	32 / MCT-0332	26	42 / MCT-0242
7	10 / MCT-0310	17	33 / MCT-0333	27	NTC - water Split
8	11 / MCT-0311	18	34 / MCT-0334	28	PTC - Split
9	12 / MCT-0312	19	25 / AGE-0466	29	TC - Split
10	NTC- water Split	20	36 / MCT-0236	30	50 bp ladder

Fig.35. Genotyping of the Tg(SftpC Luc)line6 generation 3 and 5 with list of the loaded samples. Auto exposure visualization. NTC = Negative control (nuclease free water), PTC = Positive control (SpC Luc plasmid P4 10^4), TC = Template control (transgenic negative mice sample).

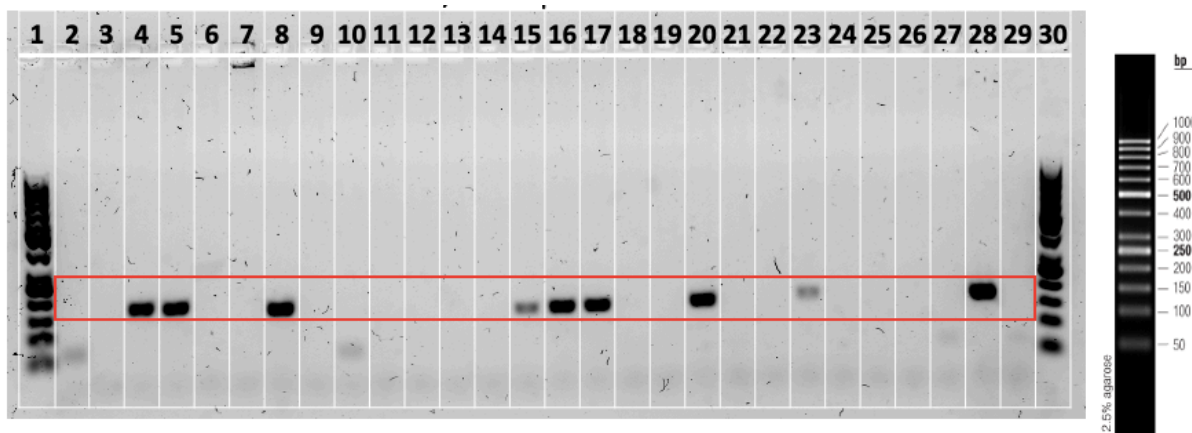


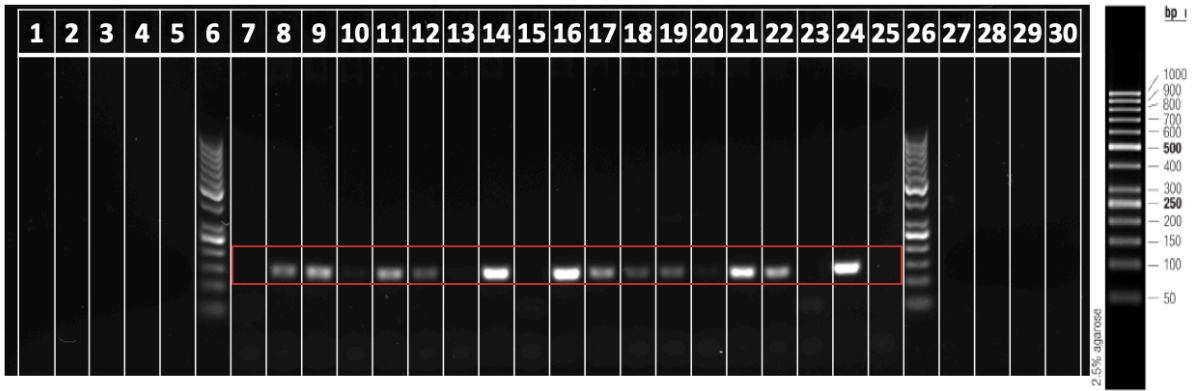
Fig.36. Genotyping of the Tg(SftpC Luc)line6 generation exposed for 3,5 sec.

Animal ID:	Run I	Run II	Run III
MCT-0306			
MCT-0307	+	++	+
MCT-0308	++	++	++
MCT-0309			
MCT-0310			
MCT-0311	=	++	=
MCT-0312			
MCT-0327			
MCT-0328			
MCT-0329			
MCT-0330			
MCT-0331		+	=
MCT-0332	++	++	++
MCT-0333	++	++	++
MCT-0334			
AGE-0466			
MCT-0236		++	++
MCT-0237			
MCT-0238			
MCT-0239	=	=	+
MCT-0240			
MCT-0241			
MCT-0242			

Fig.37. Table representing the intensity of the signals detected in each PCR run of the Tg(SftpC Luc)line6 samples. Labels legend: “++” - very high signal, “+” - high signal, “=” - low signal.

7.4.2. Genotyping of Tg(Thy1.Luc)line7

14 potentially transgenic Tg(Thy1.Luc)line7 mice were tested. The length of the amplicon is 143bp and as positive are considered all samples displayed a visible band between 100 and 150bp (Fig.37). After the three runs of the experiment 12 samples showed constant positive signal – MCT-0249(1), MCT-0250(2), MCT-0251(3), MCT-0252(4), MCT-0253(5), MCT-0255(7), MCT-0256(8), MCT-0257(9), MCT-0258(10), MCT-0259(11), MCT-0261(13), MCT-0262(14). At the plotted figure (Fig.37, Fig.38) the sample of mouse MCT-0251(3) is presented with very weak band but its intensity slightly varies at the different runs and more significant signal was detected after the repetitions of the PCR and electrophoresis procedures. The other two samples MCT-0254(6) and MCT-0260(12) displayed unconvincing signal – quite low in two of the three runs and slightly visible only at high exposure in the third run, nonetheless they could still be declared as positive. Same positive and negative controls were used for every run and they never gave false positive or false negative result. The results, in general, were well reproduced in all three runs and no significant differences were observed.



1	Loading dye	11	MCT-0252 (4)	21	MCT-0261 (13)
2	Loading dye	12	MCT-0253 (5)	22	MCT-0262 (14)
3	Loading dye	13	MCT-0254 (6)	23	NTC – water split
4	Loading dye	14	MCT-0255 (7)	24	PTC
5	Loading dye	15	NTC –water split	25	TC
6	50bp Ladder	16	MCT-0256 (8)	26	50bp Ladder
7	NTC – water split	17	MCT-0257 (9)	27	Loading dye
8	MCT-0249 (1)	18	MCT-0258 (10)	28	Loading dye
9	MCT-0250 (2)	19	MCT-0259 (11)	29	Loading dye
10	MCT-0251 (3)	20	MCT-0260 (12)	30	Loading dye

Fig.38. Genotyping of the Tg(Thy1.Luc)line7 generation 6 with list of the loaded samples. Auto exposure visualization. NTC = Negative control (nuclease free water), PTC = Positive control (Thy1.2 plasmid P4 10^4), TC = Template control (transgenic negative mice sample).

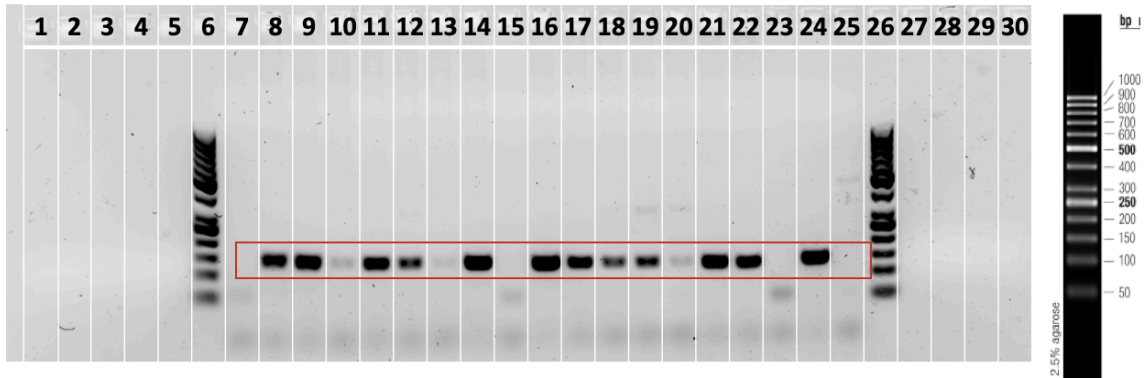


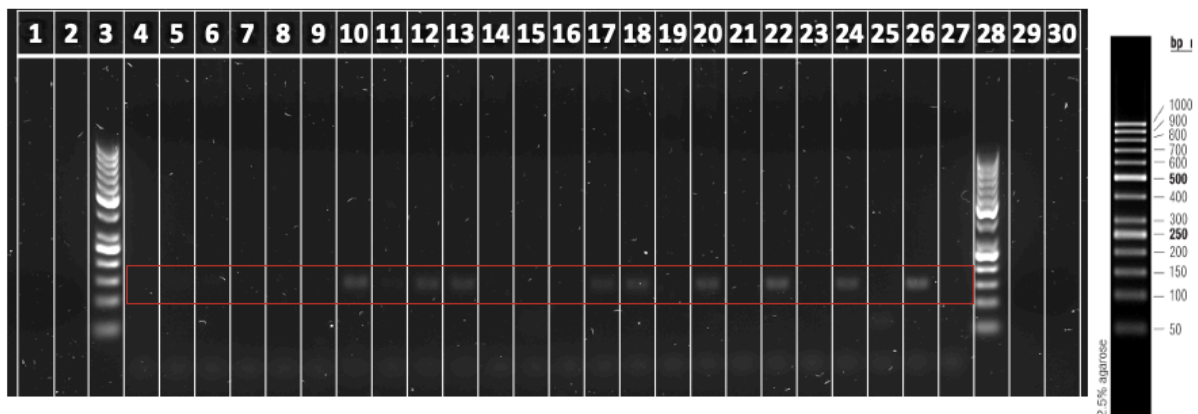
Fig.39. Genotyping of the Tg(Thy1.Luc)line7 generation 6 exposed for 3,5 sec.

Animal ID:	Run I	Run II	Run III
MCT-0249	+	+	+
MCT-0250	+	+	+
MCT-0251	=	=	=
MCT-0252	+	+	++
MCT-0253	=	+	=
MCT-0254	=		
MCT-0255	++	++	++
MCT-0256	++	++	++
MCT-0257	+	+	+
MCT-0258	+	+	=
MCT-0259	=	+	=
MCT-0260			
MCT-0261	++	++	++
MCT-0262	+	+	+

Fig. 40. Table representing the intensity of the signals detected in each PCR run of the Tg(Thy1.Luc)line7 samples. Labels legend: “++” - very high signal, “+” - high signal, “=” - low signal.

7.4.3. Genotyping of Tg(Luc705)line1050

The tested potentially transgenic mice were 19 and 7 of them were declared as positive with a visible amplicon around 150bp - MCT-0321 (21), MCT-0324 (24), MCT-0325 (25), MCT-0326 (26), MCT-0169 (69), MCT-0171 (71) and MCT-0184 (84). Sample MCT-0320(20) displayed a visible band at only one of the three runs (Fig39.) and it is not considered as transgenic since the result was not confirmed. This experiment is characterized by a significantly lower intensity of the signal with comparison to the previous two, therefore observations made on higher exposures were also used for a reliable conclusion (Fig.40, Fig.41.). At the figure which represents 6sec (Fig.41.) exposure is visible a slight signal from sample MCT-0313(13) but the mouse is not declared as transgenic because of the extremely low signal intensity and visibility only at fairly high exposures. Same positive and negative controls were used for every run and they never gave false positive or false negative result.



1	6X Loading dye	11	MCT-0319 (19)	21	MCT-0316 (16)
2	6X Loading dye	12	MCT-0324 (24)	22	MCT-0171 (71)
3	50bp Ladder	13	MCT-0321 (21)	23	MCT-0314 (14)
4	NTC- water split	14	MCT-0322 (22)	24	MCT-0184 (84)
5	MCT-0313 (13)	15	NTC - water split	25	NCT – water split
6	MCT-0183 (83)	16	MCT-0323 (23)	26	PTC
7	MCT-0315 (15)	17	MCT-0320 (20)	27	TC
8	MCT-0170 (70)	18	MCT-0325 (25)	28	50bp Ladder
9	MCT-0317 (17)	19	MCT-0318 (18)	29	Loading dye
10	MCT-0326 (26)	20	MCT-0169 (69)	30	Loading dye

Fig.41. Genotyping of the Tg(Luc705)line1050 generations 3b and 4b with list of the loaded samples. Auto exposure visualization. NTC = Negative control (nuclease free water), PTC = Positive control (SplitLuc plasmid P4 10⁴), TC = Template control (transgenic negative mice sample).

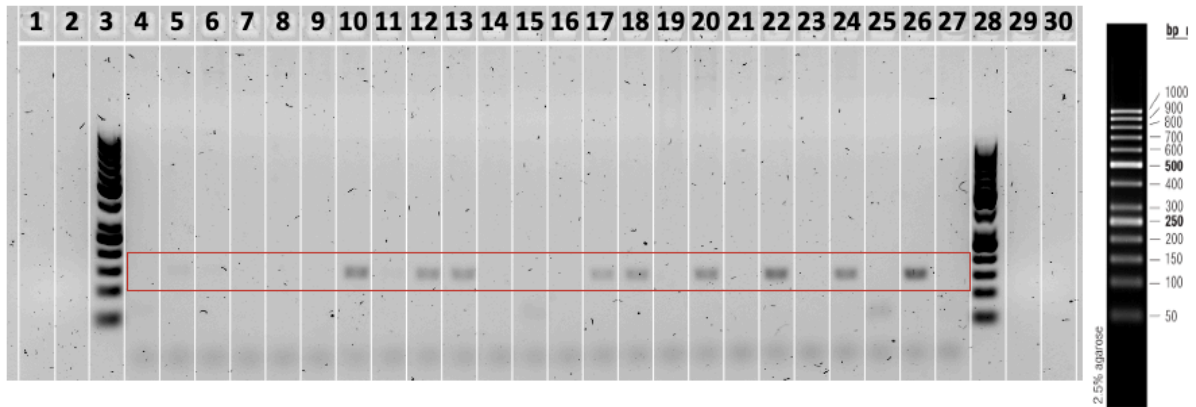
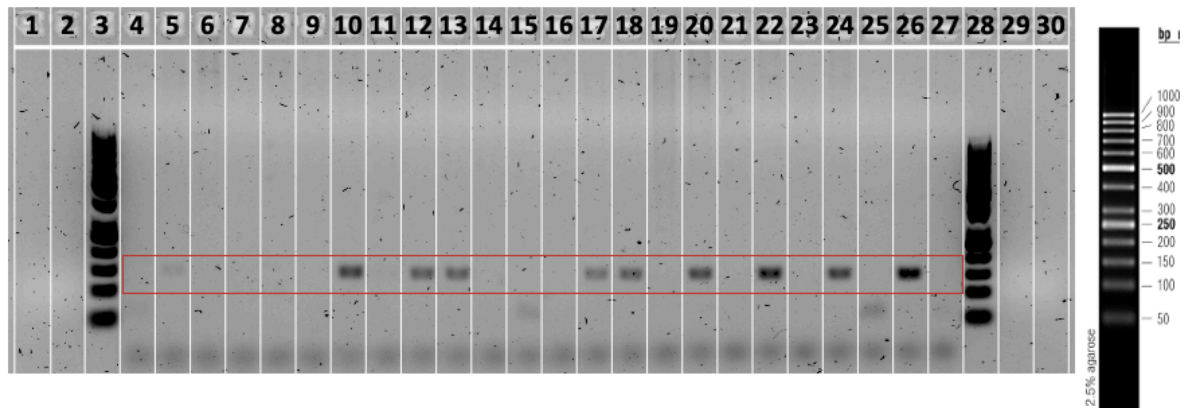


Fig.42. Genotyping of the Tg(Luc705)line1050, exposed for 4 sec.



1	6X Loading dye	11	MCT-0319 (19)	21	MCT-0316 (16)
2	6X Loading dye	12	MCT-0324 (24)	22	MCT-0171 (71)
3	50bp Ladder	13	MCT-0321 (21)	23	MCT-0314 (14)
4	NTC- water split	14	MCT-0322 (22)	24	MCT-0184 (84)
5	MCT-0313 (13)	15	NTC - water split	25	NCT – water split
6	MCT-0183 (83)	16	MCT-0323 (23)	26	PTC
7	MCT-0315 (15)	17	MCT-0320 (20)	27	TC
8	MCT-0170 (70)	18	MCT-0325 (25)	28	50bp Ladder
9	MCT-0317 (17)	19	MCT-0318 (18)	29	Loading dye
10	MCT-0326 (26)	20	MCT-0169 (69)	30	Loading dye

Fig.43. Genotyping of the Tg(Luc705)line1050 generations 3b and 4b with list of the loaded samples. Exposed for 6 sec. NTC = Negative control (nuclease free water), PTC = Positive control (SplitLuc plasmid P4 10⁴), TC = Template control (transgenic negative mice sample).

Animal ID:	Run I	Run II	Run III
MCT-0313			
MCT-0314			
MCT-0315			
MCT-0316			
MCT-0317			
MCT-0318			
MCT-0319			
MCT-0320		=	
MCT-0321	=	=	=
MCT-0322			
MCT-0323			
MCT-0324	=	=	+
MCT-0325	+	=	+
MCT-0326	=	+	=
MCT-0169	=	=	+
MCT-0170			=
MCT-0171	+	+	+
MCT-0183			
MCT-0184	=	=	+

Fig.44. Table representing the intensity of the signals detected in each PCR run of the Tg(Luc705)line1050 samples. Labels legend: “++” - very high signal, “+” - high signal, “=” - low signal.

7.5. Conclusion

The presented experiment aimed to analyse the genetic state of individuals from the offspring of three different transgenic mouse strains - Tg(SftpC Luc)line6, Tg(Thy1.Luc)line7 and Tg(Luc705)line1050, by extracting genomic DNA from ear punches, following a PCR protocol optimized beforehand and performing an agarose gel electrophoresis procedure. The total number of the tested animals is 56, of which 26 were declared transgenic. This data can be interpreted as an approximately 45% success rate of transmission of transgenicity in the generation. Considered separately, the potentially transgenic animals tested from Tg(SftpC Luc)line6 are 23 and 7 of them gave positive results, from Tg(Thy1.Luc)line7 are 14 and 12 of them gave positive results and 7 of 19 animals from Tg(Luc705)line1050 are confirmed as transgenic. The Tg(Thy1.Luc)line7 showed very satisfactory results with their significantly high percentage of transgenetically positive individuals. Whereas after PCR and electrophoresis, all samples from Tg(Luc705)line displayed amplicons with very low intensity which accordingly suggests a low level of transgene expression or mosaicism. The study was used to verify phenotypic analysis, for which no further quantitative assessment is required.

8. References:

- Badr, C. E. (2014). Chapter 1 Bioluminescence Imaging : Basics and Practical Limitations, (August). <https://doi.org/10.1007/978-1-62703-718-1>
- Badr, C. E., & Tannous, B. A. (2011). Bioluminescence imaging : progress and applications. *Trends in Biotechnology*, 29(12), 624–633. <https://doi.org/10.1016/j.tibtech.2011.06.010>
- Baert, A. L. (2008). Encyclopedia of Diagnostic Imaging. In A. L. (Editor) Baert (Ed.), *Encyclopedia of Diagnostic Imaging*. Springer, Berlin, Heidelberg. https://doi.org/https://doi.org/10.1007/978-3-540-35280-8_967
- Bauer P. (2011). *Luciferase Reporter Gene Assays. Encyclopedia of Cancer*. Springer-Verlag Berlin Heidelberg 2011. <https://doi.org/10.1007/978-3-642-16483-5>
- Chernikov, I. V, Vlassov, V. V, & Chernolovskaya, E. L. (2019). Current Development of siRNA Bioconjugates : From Research to the Clinic, *10*(April). <https://doi.org/10.3389/fphar.2019.00444>
- Choy, G., Choyke, P., & Libutti, S. K. (2003). Current Advances in Molecular Imaging : Noninvasive In Vivo Bioluminescent and Fluorescent Optical Imaging in Cancer Research, *2*(4), 303–312.
- Condeelis, J., & Weissleder, R. (2015). In Vivo Imaging in Cancer.
- Dana, H., Chalbatani, G. M., Mahmoodzadeh, H., Karimloo, R., Rezaiean, O., Moradzadeh, A., ... Gharagouzlo, E. (2017). Molecular Mechanisms and Biological Functions of siRNA, *13*(2), 48–57.
- Dunn, D. A., Kooyman, D. L., & Pinkert, C. A. (2005). Foundation Review : Transgenic animals and their impact on the drug discovery industry, *10*(11).
- Follrich, N. (2019). DIPLOMA THESIS: Near infrared imaging of bacterial ghosts and nucleic acids in vivo.

- Frederic Leblond, Scott C. Davis, P. A. V. & B. W. P. (2010). Preclinical Whole-body Fluorescence Imaging: Review of Instruments, Methods and Applications. *J Photochem Photobiol B.*, 98(1), 77–94. <https://doi.org/10.1016/j.jphotobiol.2009.11.007>. Preclinical
- Geyer, A., Lorenzer, C., Gehrig, S., Simlinger, M., Winkler, J., Sami, H., & Ogris, M. (2017). Ac ce pt cr t. *International Journal of Pharmaceutics*. <https://doi.org/10.1016/j.ijpharm.2017.02.025>
- Groza, D., Gehrig, S., Kudela, P., Holcmann, M., Pirker, C., & Dinhof, C. (2018). Bacterial ghosts as adjuvant to oxaliplatin chemotherapy in colorectal carcinomatosis, 7(5). <https://doi.org/10.1080/2162402X.2018.1424676>
- Hajam, I. A., Dar, P. A., Won, G., & Lee, J. H. (2017). Bacterial ghosts as adjuvants : mechanisms and potential. *Veterinary Research*, 1–13. <https://doi.org/10.1186/s13567-017-0442-5>
- Hong, G., Antaris, A. L., & Dai, H. (2017). Near-infrared fluorophores for biomedical imaging, (January). <https://doi.org/10.1038/s41551-016-0010>
- Huter, V., Szostak, M. P., Wanner, G., Gabor, F., Prethaler, S., & Lubitz, W. (1999). Bacterial ghosts as drug carrier and targeting vehicles, 61, 51–63.
- Ittner, L. M., & Götz, J. (2007). Pronuclear injection for the production of transgenic mice. *Nature Protocols*, 2(5), 1206–1215. <https://doi.org/10.1038/nprot.2007.145>
- Kudela, P., Juliana, V., & Lubitz, W. (2010). Bacterial ghosts (BGs)— Advanced antigen and drug delivery system. *Vaccine*, 28(36), 5760–5767. <https://doi.org/10.1016/j.vaccine.2010.06.087>
- Langemann, T., Koller, V. J., Muhammad, A., Kudela, P., Mayr, U. B., & Lubitz, W. (2010). The bacterial ghost platform system Production and applications, 1(5), 326–336. <https://doi.org/10.4161/bbug.1.5.12540>

- Lee, P. Y., Costumbrado, J., Hsu, C., & Kim, Y. H. (2012). Agarose Gel Electrophoresis for the Separation of DNA Fragments, (April), 1–5. <https://doi.org/10.3791/3923>
- Leung, R. K. M., & Whittaker, P. A. (2005). RNA interference : from gene silencing to gene-specific therapeutics, *107*, 222–239. <https://doi.org/10.1016/j.pharmthera.2005.03.004>
- Lubitz, W. (2001). Bacterial ghosts as carrier and, 765–771.
- Mader, H. J., Szostak, M. P., & Haslberger, A. G. (1997). Endotoxicity does not limit the use of bacterial ghosts as candidate vaccines, *15*(2), 195–202.
- Mader, R. M., Müller, M., & Steger, G. G. (1998). Resistance to 5-fluorouracil. *General Pharmacology*, *31*(5), 661–666. [https://doi.org/10.1016/S0306-3623\(98\)00191-8](https://doi.org/10.1016/S0306-3623(98)00191-8)
- Mansoori, B., Shotorbani, S. S., & Baradaran, B. (2014). RNA Interference and its Role in Cancer Therapy, *4*(4), 313–321. <https://doi.org/10.5681/apb.2014.046>
- Mármol, I., Sánchez-de-diego, C., Dieste, A. P., Cerrada, E., Jesús, M., & Yoldi, R. (n.d.). Colorectal Carcinoma : A General Overview and Future Perspectives in Colorectal Cancer. <https://doi.org/10.3390/ijms18010197>
- National Laboratory of Enteric Pathogens, Bureau of Microbiology, L. C. for D. C. (1991). The polymerase chain reaction: An overview and development of diagnostic PCR protocols at the LCDC. *Can J Infect Dis.*, 89–91. <https://doi.org/10.1155/1991/580478>
- Paukner, S., Kohl, G., & Lubitz, W. (2004). Bacterial ghosts as novel advanced drug delivery systems : antiproliferative activity of loaded doxorubicin in human Caco-2 cells, *94*, 63–74. <https://doi.org/10.1016/j.jconrel.2003.09.010>
- Paukner, S., Stiedl, T., Kudela, P., Bizik, J., Laham, F. Al, & Lubitz, W. (2006). Bacterial ghosts as a novel advanced targeting system for drug and DNA delivery, 11–22.
- Pinczolits, S. (2017). DIPLOMARBEIT / DIPLOMA THESIS Titel der Diplomarbeit / Title of the Diploma Thesis transgenic reporter mouse strains “.

- Resina, S., Turner, J. J., Prevot, P., Travo, A., Clair, P., Gait, M. J., ... Lebleu, B. (2007). Lipoplex and peptide-based strategies for the delivery of steric-block oligonucleotides, *344*, 96–102. <https://doi.org/10.1016/j.ijpharm.2007.04.039>
- Riedmann, E. M., Kyd, J. M., Cripps, A. W., & Lubitz, W. (2007). Bacterial ghosts as adjuvant particles, 241–253.
- Sadikot, R. T., & Blackwell, T. S. (2005). Bioluminescence Imaging. *Proc Am Thorac Soc*, *2*(28), 537–540. <https://doi.org/10.1513/pats.200507-067DS>
- Schochetman, G., Ou, C., & Jones, W. K. (1988). Polymerase Chain Reaction. *THE JOURNAL OF INFECTIOUS DISEASES*, *158*(6), 1154–1157.
- Schön, P., Schrot, G., Wanner, G., Lubitz, W., & Witte, A. (1995). Two-stage model for integration of the lysis protein E of @ X174 into the cell envelope of Escherichia coli, *17*, 207–212.
- Singh, A., Trivedi, P., & Jain, N. K. (2018). Advances in siRNA delivery in cancer therapy. *Artificial Cells, Nanomedicine, and Biotechnology*, *0*(0), 274–283. <https://doi.org/10.1080/21691401.2017.1307210>
- Stuker, F., Ripoll, J., Rudin, M., & Vouton, V. (2011). Potential for Pharmaceutical Research, 229–274. <https://doi.org/10.3390/pharmaceutics3020229>
- Tseng, J.-C., Vasquez, K., & Peterson, J. (2015). Optical Imaging on the IVIS SpectrumCT System : General and Technical Considerations for 2D and 3D Imaging, (1), 1–18.
- Wheeler, M. B., Walters, E. M., & Clark, S. G. (2003). Transgenic animals in biomedicine and agriculture : outlook for the future. *Animal Reproduction Science*, *79*, 265–289. [https://doi.org/10.1016/S0378-4320\(03\)00168-4](https://doi.org/10.1016/S0378-4320(03)00168-4)
- Yan, Y., Shi, P., Song, W., & Bi, S. (2019). T h e r a n o s t i c s Chemiluminescence and Bioluminescence Imaging for Biosensing and Therapy : In Vitro and In Vivo

Perspectives, 9(14). <https://doi.org/10.7150/thno.33228>

Youssof, A. M. E., Alanazi, F. K., Salem-bekhit, M. M., Shakeel, F., & Haq, N. (2019). Bacterial Ghosts Carrying 5-Fluorouracil : A Novel Biological Carrier for Targeting Colorectal Cancer. *AAPS PharmSciTech*, 20(48), 1–12. <https://doi.org/10.1208/s12249-018-1249-z>